

**Radiation and Eddy Flux Experiment 1993
(REFLEX II)**

**Christoph Kottmeier, Jörg Hartmann,
Christian Wamser, Axel Bochert,
Christof Lüpkes, Dietmar Freese,
and Wolfgang Cohrs**

**Ber. Polarforsch. 133 (1994)
ISSN 0176 - 5027**

Christoph Kottmeier
Jörg Hartmann
Christian Wamser
Axel Bochert
Christof Lüpkes
Dietmar Freese
Wolfgang Cohrs

Alfred-Wegener-Institut für Polar- und Meeresforschung
Columbusstraße
D-27515 Bremerhaven
Bundesrepublik Deutschland

Contents

Abstract	iv
1 Introduction	1
2 The <i>Polar 2</i> and <i>Polar 4</i> Aircraft Instrumentation	3
2.1 Dropsonde system	4
2.2 Laser Altimeter	4
2.3 The line scan systems	4
3 Experimental Phase	7
4 Sensor Calibration and Intercomparison	9
4.1 Sensor calibrations	9
4.2 Flight comparisons	12
4.3 Comparison flight between <i>Polar 2</i> and <i>D-IBUF</i>	13
4.4 Dropsonde and aircraft intercomparison	16
5 Flight Catalogue	19
6 Data Presentation	45
6.1 Detection of surface structure by laser altimeter measurements	45
6.2 Observations with the Line Scanner Systems	46
6.3 Observation of mesoscale atmospheric structures	49
6.4 Comparison of ERS I SAR-data and digital camera data	57
7 References	61
8 Acknowledgements	62

List of Figures

1	KT4 correction	9
2	Longwave radiation fluxes after recalibration	11
3	Radiation intercomparisons	12
4	Intercomparison flight path.	13
5	Comparison of temperature and humidity.	14
6	Comparison of the gps-corrected wind vector.	16
7	Comparison of temperature and relative humidity	17
8	Wind intercomparison	18
9	NOAA 11, 11:52:45, Polar 4 track.	20
10	NOAA 12, 08:42:00, Polar 4 track.	22
11	NOAA 12, 08:21:00, Polar 2 track.	24
12	NOAA 11, 12:49:16, Polar 4 track.	26
13	NOAA 11, 11:52:45, Polar 4 track.	28
14	NOAA 11, 12:26:13, Polar 2 track.	30
15	NOAA 10, 09:21:00, Polar 4 track.	32
16	NOAA 10, 08:57:00, Polar 2 track.	34
17	NOAA 11, 12:41:24, Polar 4 track.	36
18	NOAA 11, 12:29:44, Polar 4 track.	38
19	NOAA 11, 11:52:45, Polar 4 track.	40
20	NOAA 11, 06:26:00, Polar 4 track.	42
21	An example of laseraltimeter and KT4-data	46
22	An example of LSC and IRLS-images	47
23	Ice types from LSC and IRLS-data	48
24	Profiles on March 4	50
25	Profiles on March 10	51

26	Profiles on March 11	52
27	Box flight pattern	53
28	Wind profiles on 25 March	54
29	Temperature profiles on 25 March	55
30	Humidity profiles on 25 March	56
31	NOAA-11 image on March 12	58
32	SAR-, LSC- and IRLS-images on March 12	59
33	LSC- and IRLS-images near POLARSTERN	60

List of Tables

1	Instruments of Polar 2 and Polar 4	3
2	Laser Altimeter Technical Specifications	4
3	Technical details of the Line Scan Cameras.	5
4	Calibration coefficients of radiation sensors.	10
5	Comparison of turbulence statistics.	15

Abstract

REFLEX II was a winter study of interactions between the sea ice covered ocean and the atmospheric boundary layer in the marginal ice zone north of Svalbard (15°E 78°N). The experiment was based on flights of the aircraft *Polar 2* and *Polar 4* between February 28 and March 25, 1993. It was conducted simultaneously with the experiment ARKTIS 93, which comprised the missions of two other aircraft, of RV *POLARSTERN* and two other ships.

The polar aircraft were equipped with basic meteorological and radiation instruments. *Polar 2* also carried scanning cameras in the visible and thermal infrared to detect the ice and new ice (nilas) concentrations and the surface temperature with a spatial resolution of $\approx 4\text{ m}^2$. A turbulence probing system and a laser altimeter on the same aircraft provided coincident data on the surface structure and on turbulence and turbulent fluxes in the atmospheric boundary layer. *Polar 4* was equipped with a dropsonde system. A total of 23 flights on 12 days were performed under prevailing very cold weather conditions. The flights were arranged to study the effects of different ice conditions on the low-level turbulence and the radiation flux regime over sea ice in the presence of low clouds. The surface structure was recorded by the cameras in those regions, where on the same day SAR-scenes of the ERS-I were obtained. Forcing and validation data sets for mesoscale modelling work were achieved by tightly coordinated aircraft missions over the marginal ice zone.

This report briefly outlines the scientific objectives and describes the instrumentation and the experimental phase. It comprises a catalogue of all flights and presents examples of typical features measured during the campaign.

1. Introduction

The *Radiation and Eddy Flux Experiment*, REFLEX II, was conducted to the north and west of Svalbard (15°E 78°N) on the basis of measurements with the two aircraft *Polar 2* and *Polar 4* of the Alfred Wegener Institute. REFLEX II was a winter experiment with scientific objectives similar to those of the REFLEX I experiment in 1991 (Hartmann et al., 1992).

It aims to study atmospheric processes affected by Arctic sea ice during wintertime. Since the vertical exchange of momentum and energy vary considerably with ice concentration, ice thickness and floe size distribution, a major objective of the programme is to derive schemes, which parameterise turbulent fluxes in relation to sea ice statistics. In wintertime with prevailing very low air temperatures the extent of leads or thin ice in contact with the air is particularly important for the heat exchange. Therefore turbulent fluxes of heat, humidity and momentum are determined from aircraft data and related to floe size and surface temperature statistics from scanning camera systems.

The turbulent exchange of heat, momentum and moisture plays a key role in the formation of low stratus clouds, which in turn, influence the surface radiation balance. Flight patterns of *Polar 2* and *Polar 4* were arranged to obtain data on cloud shortwave transmissivity and cloud longwave emissivity. During cold air outbreaks, south of the sea ice region convection frequently organises into vortex rolls. As a supplement to the related aircraft missions of the coincident experiment ARKTIS 93 wind, temperature and humidity were determined from dropsonde profiles along the air mass trajectories over the open ocean.

The state of the lower atmosphere in the vicinity of the ice margin was determined by frequent *Polar 4* ascents/descents and dropsonde profiles, while *Polar 2* obtained the energy fluxes on a scale of 100 km x 100 km. The data will be used for the forcing and validation of mesoscale model studies with a 3 D nonhydrostatic model (METRAS).

With considerable effort the aircraft missions were arranged to obtain ground truth data for the interpretation of data from the SAR-instrument (Synthetic aperture radar) flown onboard the ERS-I (European Research Satellite). The airborne information comprise the surface temperature, ice concentration and geometric surface roughness.

The aircraft instrumentation basically has been described in the REFLEX I experiment report. The present report covers the new instruments on the aircraft and important items with respect to calibration and intercomparison in sections 3 and 4. A catalogue of flights with flight patterns and NOAA satellite images is given in section 5. Examples of data elucidating their suitability to the scientific objectives are presented in section 6.

2. The *Polar 2* and *Polar 4* Aircraft Instrumentation

The *Polar 2* and *Polar 4* are Dornier DO228 turbo-prop aircraft with a wing span of 17m and a length of 15m. They are fully IFR-equipped and have laser-gyro Inertial Navigation Systems (INS). For REFLEX II separate Global Positioning Systems (GPS) were available for the pilots for precise navigation and for scientific purposes. Generally, missions were flown with a five person crew, two pilots, one or two operators and one or two scientists.

During REFLEX II the *Basic Meteorological Facilities*, the *Meteopod* turbulence system, the *Visible Line Scan Camera* were flown on the *Polar 2* aircraft, while the *Dropsonde* system was transferred to the *Polar 4*. These instruments were briefly described in the experiment report on REFLEX I (Hartmann et al., 1992) and have not been modified significantly. Additional instrumentation systems of REFLEX II are described below. Table 1 lists a summary of the instrumentation.

Table 1: Instruments of *Polar 2* and *Polar 4* during REFLEX II.

Polar 2 and Polar 4	
sensor	model
static pressure	Rosemount 856AE13 (de-iceable)
absolute pressure	Rosemount 1201F2A1B1B
differential pressure	Rosemount 1221F2VL6B1B
temperature (PT 100)	Rosemount 102 EJ 2BB
humidity	Aerodata AD-FS-88 (Vaisala Humicap and PT 100)
2 pyranometers (up/down)	Eppley PSP
2 pyrgeometers (up/down)	Eppley PIR
radiation thermometer	Heimann KT 4
GPS-positioning	SEL 6-channel
INS-positioning	Honeywell Lasernav
only Polar 2	
5-hole-probe	Rosemount 858AJ28
temperature	AWI Pt 100 reverse-flow housing
absolute pressure	Rosemount 1201F2A
differential pressure	Rosemount 1221F2
fast humidity (Lyman- α)	Atm.Instr.Res. AIR-LA1
absolute humidity	General Eastern 1011B reverse-flow
inertial-platform	dew-point-mirror Litton LTR-81
Line Scan Camera (VIS)	AWI
Line Scan Camera (IR)	AWI
laser-altimeter	IBEO PS 100 0-100m, 2 cm resolution, 2000 Hz
radar-altimeter	TRT AHV-20, 0-1500m, 0.3 m resolution, 50 Hz
only Polar 4	
dropsonde system	Vaisala/Aerodata Marwin MW12C

2.1. Dropsonde system

During REFLEX II the Vaisala Marwin MW12c radio sonde system was used with major modifications in comparison to REFLEX I, where no valuable wind data could be obtained. A new Motherboard MPU 13 and a new software, version number 5.13, capable of including Loran-C and Navy-VLF stations in the wind calculation, were installed. Further modifications included the sonde antenna and an antenna amplifier and the aircraft antenna. With these modifications the dropsondes yielded acceptable wind data. In section 4 a comparison with the aircraft wind measurements is shown.

2.2. Laser Altimeter

To record the structure of the ice surface on a centimetre scale, Polar 2 carried a vertically downward looking laser altimeter. The distance measuring is based on reflection of the laser beam from a natural surface. Measurements require a high albedo and are not possible over water, when the aircraft height is 30 m.

Table 2: Laser Altimeter Technical Specifications

type:	PS 100 E, manufacturer: IBEO, Hamburg
power:	100 W
range:	100 m over a white surface
lens diameter:	42 mm
beam divergence:	2.4 mrad
pulse frequency:	2 000 Hz
pulse duration:	10 ns
wavelength:	905 nm
distance accuracy:	3 cm for a single pulse on white surface
footprint size:	11.4 cm for an aircraft height of 30 m

The instrument was operated at a pulse frequency of 2 000 Hz. With the typical aircraft speed of 70 m/s this corresponds to 3.5 cm horizontal distance between pulses. The laser beam has a divergence of 2.4 mrad leading to a diameter of 11 cm at 30 m, the typical aircraft height during measuring runs. The standard error for a target distance of 30 m is 3 cm. Since individual pulses are independent, averaging over 3 consecutive measurements reduces the standard error of the mean distance to 1.7 cm. Table 2 summarises the specifications of the instrument.

2.3. The line scan systems

Two different digital line scan systems were installed on *Polar 2*. Both instruments consist of cross-track scanners to measure the intensity of surface signals perpendicular to the flight track, one in the visible and the other in the infrared range.

The altitude of the aircraft determines the width and cross-track resolution of the images. Since the scanners enable the sampling of 50 lines per second, the along-track resolution is determined by the aircraft's ground speed and with a typical aircraft speed of 70 m/s is about 1.5 m.

Table 3: Technical details of the Line Scan Cameras.

system parameters	LSC	IRLS
sensor	CCD 512 pixels	single IR sensor at 77 K
wavelength band	0.4 μm - 1.1 μm	8 μm - 12 μm
optics	8 mm lens, f/1.4	rotating mirror, f/1.1
scan angle	90°	90°
temporal resolution	50 scans / s	50 scans / s
cross flight track resolution at a flight altitude of 500 m	2 m	2 m (average)
along flight track resolution for an aircraft speed of 70 m/s	1.4 m	1.4 m
sensitivity	256 gray levels	0.1 K (25 K range)
quantities to be derived from data	concentration of ice nilas and open water, ice floe size distribution; surface roughness	structural details of ice floes. surface temperature distribution, ice types

Ice, nilas and water concentrations can be derived from data of the vertically downward looking visible Line Scan Camera (LSC) which is sensitive in the visible and near infrared spectral range of 400 - 1100 nm. It observes the reflectance of the sea surface elements. High resolution data of the surface temperature were measured by means of an Infrared Line Scanner (IRLS). The sensor operates in the thermal infrared range between 8 μm and 12 μm which covers an adjustable temperature range of 25 K with a resolution of 0.1 K. This system was operated (after some test flights in the Antarctic) for the first time routinely during REFLEX II. Both the LSC and the IRLS scan the same area beneath the aircraft and were adjusted to similar spatial resolution. Some technical details of the systems are summarized in Table 3.

3. Experimental Phase

The experiment took place from February 28th to March 25th, 1993. During the missions, the instruments were operated by scientists of the Alfred-Wegener-Institut für Polar- und Meeresforschung (AWI) and engineers of *Aerodata GmbH*, Braunschweig. The *Polar 2* and *Polar 4* were flown by pilots of the *Deutsche Forschungsanstalt für Luft- und Raumfahrt* (DLR) and *Aerodata*.

REFLEX II was conducted simultaneously with the experiment ARKTIS 93. ARKTIS 93 comprised missions of the aircraft D-IBUF (Do 128) and FALCON from the same base. Within the same experiment three research vessels were present in the region. RV POLARSTERN took a position in the marginal sea ice zone at about 81 °N, 5 ° E, while Valdivia and Professor Multanovsky performed observation programs between 70 °N and 75 °N.

All flights were planned in a temporary office of the *Norsk Polar Institutt* at Longyearbyen Lufthavn. Weather information was available from the meteorologist of *Det Norske Meteorologiske Institutt* (DNMI) at Longyearbyen and from maps received by fax. Actual satellite information from NOAA satellites were transmitted via telecommunication link from TSS (Trömsø Satellite Station) and by means of a small satellite receiving station. Additional weather information was available from the ships.

All aircraft operations took place in the area to the west and north of Svalbard between 0 °E, 78 °N and 20 °E, 82°N. The catalogue of flights (Section 5) shows the individual flight paths.

Flight patterns belonged to one of the following basic types:

- I Low level flights of POLAR 2 at an altitude of 30 m for studies of turbulent fluxes of momentum, heat and moisture above different ice categories. LSC, IRLS and Laser altimeter data are also available for most of these low level flights.
- II Flight patterns of both aircraft with frequent aircraft ascents/descents and dropsonde releases on a horizontal scale of 100 km x 100 km for the documentation of mesoscale structures in marginal ice zone.
- III Line Scan camera (LSC) and Infrared Line Scanner (IRLS) survey flights for studies of ice type distribution, concentration, floe size and surface temperature distribution.
- IV POLAR 2 and POLAR 4 flights, coordinated to observe the effects of low level clouds on the surface radiation balance and on the net radiation of the cloud/sea ice system.
- V POLAR 4-flights with dropsonde releases to document the modification of the air mass during cold air outbreaks over the ocean.

Patterns I were flown over distances of 20 to 50 km in the sea ice region and organized to cover a wide range of ice concentrations and thermal stratification. They were repeated several times in order to obtain reliable turbulence statistics. While

POLARSTERN was in the sea ice, several flight sections for the intercomparison of aircraft and ground data were flown. Turbulence data at the levels of 30 m and 60 m are available for total flight lengths of 3075 km and 260 km respectively.

The mesoscale patterns II were flown as boxes over the ice margin on 4 days and as distance/height cross sections during cold air outbreaks on 3 days. The patterns and measurements of the boxes were arranged to provide a good horizontal and vertical resolution and to obtain relevant parameters for the forcing and validation of mesoscale atmospheric models.

The flights III with the LSC and IRLS were performed on 11 days. On 9 days the surface was observed in regions, which were also covered by scenes of the Synthetic Aperture Radar (SAR) onboard the European Research Satellite (ERS I).

Patterns IV included *Polar 2* and *Polar 4* intercomparisons in loose formation flights (5 legs) and intercomparisons with the ground observations at the KOLDEWEY-Station in Ny-Alesund (Svalbard) (5 legs) and at POLARSTERN (15 legs). The shortwave and longwave flux differences across the atmospheric boundary layer caused by low-level cloud decks were determined by *Polar 2* and *Polar 4* flight at different heights (11 legs). The aircraft ascents (120 profiles) provided vertical profiles of radiative fluxes, temperature and humidity and cloud thickness information.

The flights according to pattern V were performed from approximately 350 km downstream of the ice margin to a position 100 km upstream of the ice margin at a flight level of 3000 m with dropsondes released every 10 min. The dropsonde temperature, humidity and wind data on three occasions document modifications along the air mass trajectory and serve as a contribution to the related D-IBUF- and FALCON-missions during cold air outbreaks.

4. Sensor Calibration and Intercomparison

4.1. Sensor calibrations

4.1.1. Radiation Thermometer

During nine flights the KT4-radiation measurements onboard *Polar 2* were calibrated with a black body radiator moved into the optical path. The black body temperatures cover the temperature range from -27 and $+5^\circ\text{C}$. The temperatures of the radiation thermometer show a systematic deviation from those of the black body, which can be described by

$$T_{KT4,c} = -1.524 \cdot 10^{-6} T_{KT4,m}^4 - 1.455 \cdot 10^{-4} T_{KT4,m}^3 - 1.1 \cdot 10^{-5} T_{KT4,m}^2 + 0.901 T_{KT4,m} + 1.305 \text{ K}, \quad (1)$$

where $T_{KT4,m}$ denotes the observed and $T_{KT4,c}$ the corrected surface temperature, both in $^\circ\text{C}$. The standard deviation of the calibration points from the regression polynomial is 0.5 K.

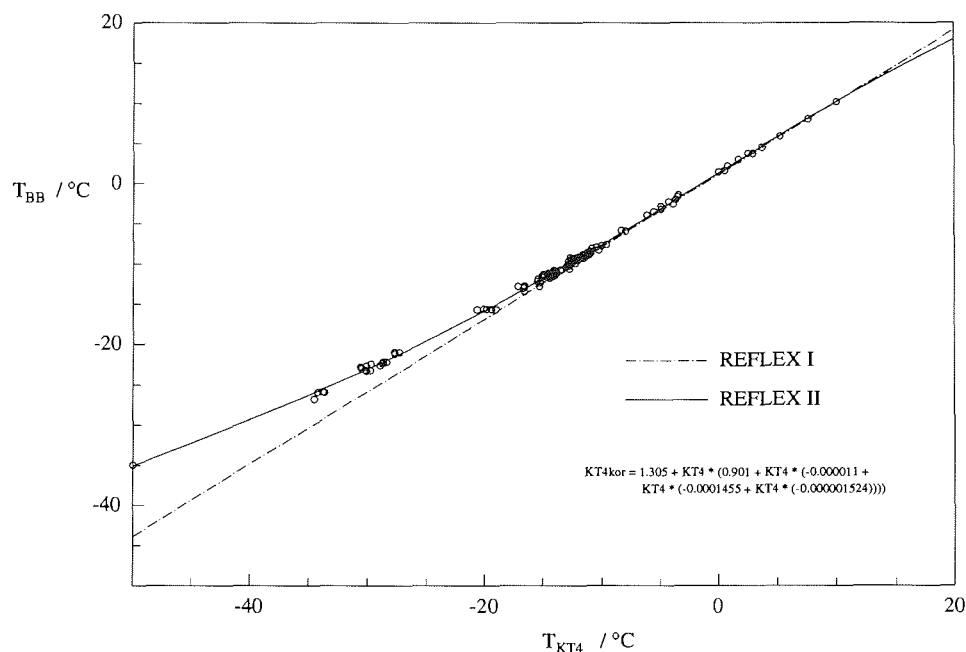


Figure 1: KT4 correction based on black body calibrations.

The correction fits well with the linear REFLEX I calibration, where the black body temperature was not below -12°C . The observed $T_{KT4,m}$ during REFLEX II are

frequently below -35°C over sea ice. Since no calibration data at such low temperatures are available, the polynom used for correction (see Figure 1) becomes uncertain to $\pm 1 - 2\text{ K}$ below -40°C .

4.1.2. Recalibration of radiation sensors

The four pyrgeometers and four pyranometers of the aircraft since 1988 have been regularly calibrated at the ‘‘Meteorologisches Observatorium des Deutschen Wetterdienstes’’ (DWD) once per year since 1988. The calibration protocols from 1988 to 1993 are used to determine variations of the sensitivities and offsets of the instruments.

The calibration coefficients of the pyranometers are very stable throughout the period (see Table 4). No modifications are applied to the REFLEX II-data.

$$F_l = V_{th}/R + \sigma T_s^4 + K\sigma(T_s^4 - T_d^4)$$

		pyrgeometer sensitivity R in mV/W m^{-2}			
		PIR 26955 F3	PIR 26956 F3	PIR 26810 F3	PIR 26811 F3
		Polar2 FL↓	Polar2 FL↑	Polar4 FL↓	Polar4 FL↑
calibration at					
	March 30,1989			35.8	34.4
DWD	April 23,1990			38.3	36.7
Meteorologisches	June 4,1991		35.6		
Observatorium	August 1,1991	35.3			
Hamburg	January 21,1993	35.5	34.2	38.1	35.8
	June 10,1993		34.4	35.1	34.4
	July 6,1993	33.7			
recalibration					
	R in mV/W m^{-2}	32.5 ± 1.0	31.5 ± 0.5	33.5 ± 1.0	34.0 ± 0.5
	K	3.0 ± 1.5	5 ± 1	4 ± 1	3 ± 1

Table 4: Calibration coefficients of radiation sensors.

The pyrgeometers are recalibrated on the basis of a method slightly different to that applied by the DWD. According to Albrecht et al. (1975) the longwave radiation flux F_l is determined by the sensor heat budget components via the relation

$$F_l = \frac{1}{R} U_{th} + \sigma T_c^4 - K\sigma(T_d^4 - T_c^4), \quad (2)$$

where R is the sensitivity of the thermopile, U_{th} is the voltage of the thermopile, σ is the Stefan-Boltzmann constant ($\sigma = 5.66 \cdot 10^{-8} \text{ W}/(\text{m}^2 \text{K}^4)$), T_c and T_d are the thermopile sink temperature and the dome temperature respectively, K is a coefficient defined as the ratio between the emissivity of the inside of the dome and the dome transmissivity.

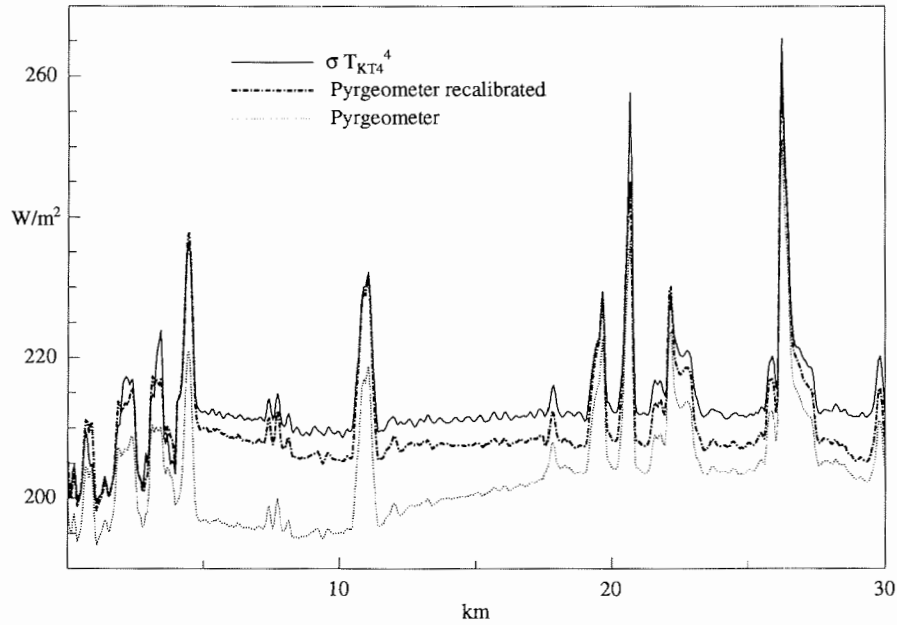


Figure 2: .

Longwave radiation fluxes before and after recalibration. The KT4-signal is low-pass filtered to correct for the hemispheric view of the pyrgeometer.

The DWD-method assumes, that T_c and T_d are the same, which causes the last term to vanish. Inspection of the temperatures shows, however, that they differ and the coefficients R and K of the above equation are calculated by a least squares method for each calibration run. The results are given in Table 4. The parameter K is characteristic for the dome and is of the same magnitude found during other studies (Albrecht et. al, 1975). The improvement of the new calibration is obvious from Figure 2.

The downward looking pyrgeometer of POLAR 2 is compared to the KT4 data during flights at a level of 30 m. The longwave radiation flux observed by both instruments then is

$$F_l^{\dagger} = \epsilon \sigma T_0^4, \quad (3)$$

since the emission of the intermediate thin and dry atmospheric layer is weak. KT4 temperatures have been averaged with respect to the hemispheric view of the pyrgeometer and were applied for flight calibration. Based on the above equation, the estimated parameters R and K are close to the laboratory results.

4.2. Flight comparisons

During the course of REFLEX II intercomparisons were performed between different sensors onboard the aircraft and between aircraft and ground sensors.

4.2.1. Comparison of radiation fluxes

The radiation sensors of *Polar 2* and *Polar 4* were compared on 9 flight legs, while the aircraft flew in loose formation. Aircraft radiation data were compared with ground data obtained during low level overflights of the Baseline Surface Radiation Network Station (BSRN) at the Koldewey-Station (Ny Alesund) and of the radiation instruments near RV POLARSTERN.

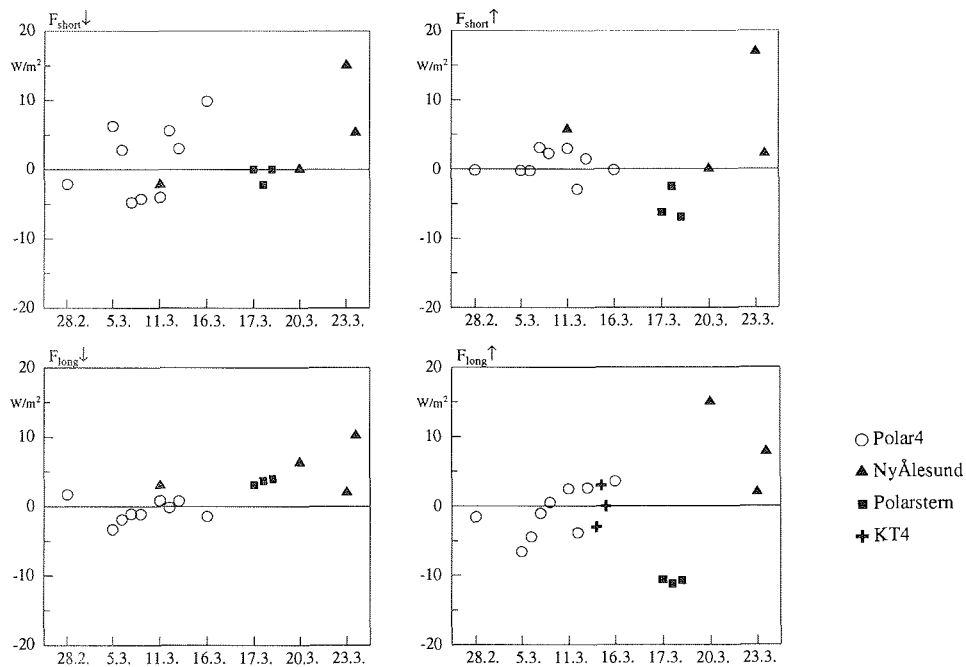


Figure 3: Summary of radiation intercomparisons during REFLEX II. All data refer to *Polar 2*.

Figure 3 shows the mean offsets of instruments from all comparison flights. The differences of both longwave hemispheric fluxes and of the upwelling shortwave fluxes between *Polar 2* and *Polar 4* are smaller than $\pm 5 W/m^2$. The global radiation data differ within $\pm 10 W/m^2$, which is mainly due to the aircraft separation and effects of high clouds during the flights. The difference is smaller for flight legs under close formation. The downwelling fluxes measured near POLARSTERN hardly deviate from the aircraft data. Offsets of $5 - 10 W/m^2$ are found for the upwelling fluxes,

since the ship observations reflect the local effects beneath the sensors. The radiation data at the Koldewey-Station are obtained within horizontally heterogeneous surroundings and were averaged over 5 min.

4.3. Comparison flight between *Polar 2* and *D-IBUF*

On March 4 the instruments of the *Polar 2* and of the *DO 128 (IBUF)* of the Institut für Flugführung, Universität Braunschweig, were compared.

4.3.1. Flight track

After take off in Longyearbyen *Polar 2* and *D-IBUF* flew at 200 ft over the partly ice-covered Isfjord to the west. *IBUF* lead and *Polar 2* followed in about an 8 o'clock position. At the exit of the fjord, both aircraft turned to the north and ascended to 3000 m. Figure 4 shows a plot of the flight path. Sections used for intercomparison are marked by a bold line.

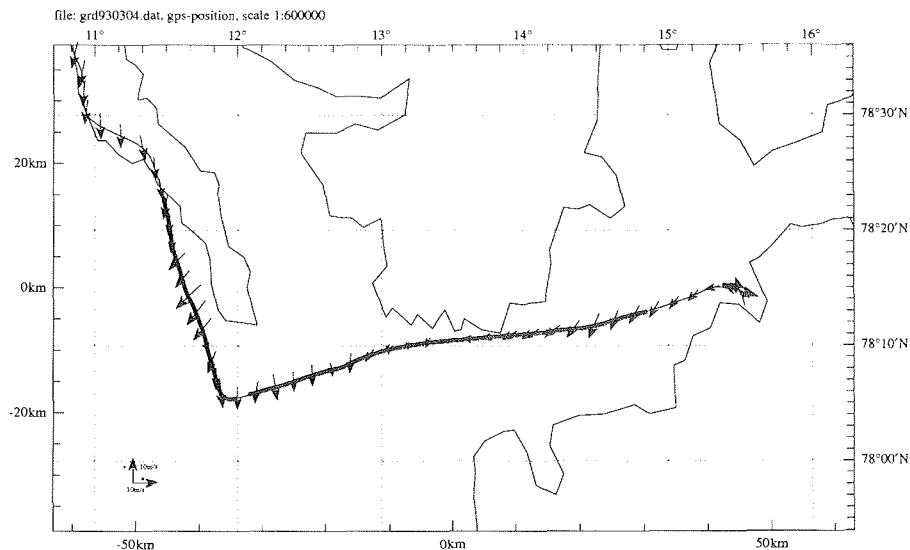


Figure 4: Intercomparison flight path of the *Polar 2* and *D-IBUF*.

4.3.2. Pressure, temperature and humidity

For both aircraft the potential temperature θ and the specific humidity q during the ascent are plotted versus height in Figure 5. The height is calculated by integration of the barometric formula with the actual temperature measurements.

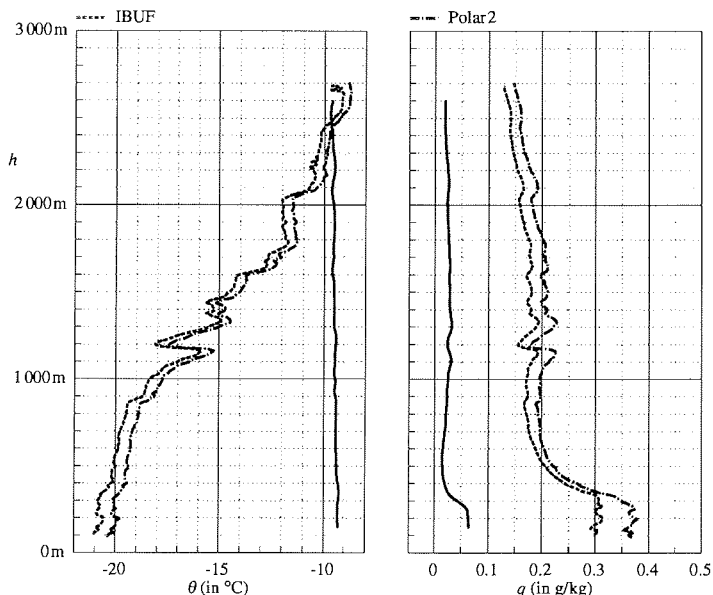


Figure 5: Comparison of temperature and humidity.

Before takeoff the static pressures of the aircraft differed by 5.7 hpa. Interference with the running engines may contribute to this large value. A vertical alignment of significant features in the soundings reveals a pressure difference of 3 hpa. This value coincides with the specified accuracy of the Meteopod pressure transducer.

The temperature measurements (channel 29 of IBUF and channel 45 of Polar 2) differ by 0.7 K, at the beginning of the ascent and by 0.4 K at the end. The difference between the specific humidity, measured with a Vaisala Humicap, is between 0.025 and 0.05 g/kg.

4.3.3. Wind vector

Comparisons of the wind vector measurements are shown in Figure 6. It shows a good agreement in the u -component. As the flight was on a northbound track, this component is approximately orthogonal to the longitudinal axis of the aircraft. However, a large difference increasing from 1 m/s at the beginning to 2 m/s at the end of the ascent appears in the v -component. This difference mainly results from INS data of the aircraft velocity in the earth-system, since the airspeed measurements agreed very well. The INS error is caused by Schuler oscillations which vary in phase and amplitude for both aircraft. By using data from the gps-receivers carried in both aircraft, a first order correction can be applied: long term variations of the aircraft velocity component are removed from the INS data and replaced by the correspondingly low-pass filtered GPS data. The corrected wind measurements, shown in Figure 6, agree now on average within 0.5 m/s.

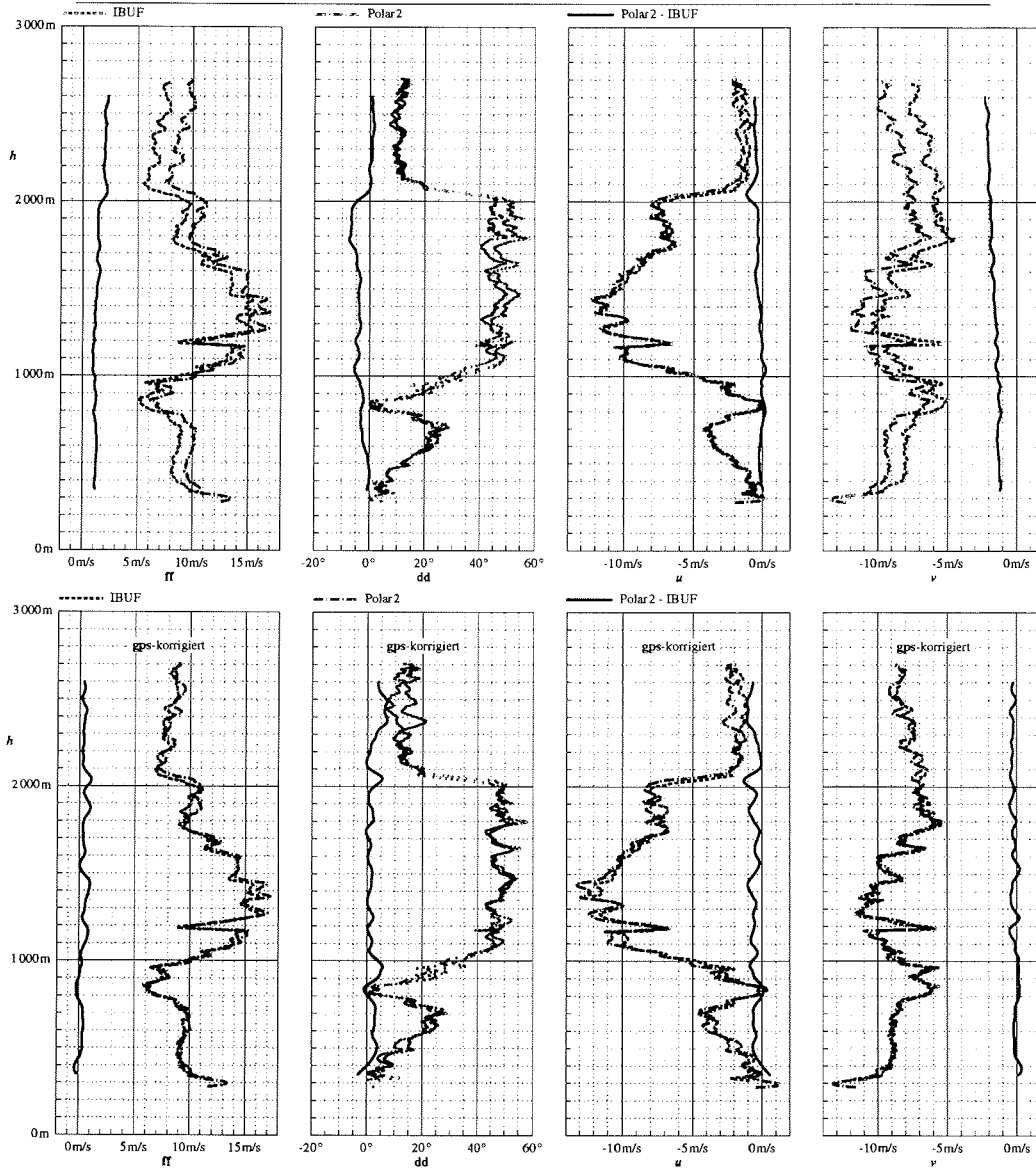


Figure 6: Comparison of the uncorrected (top) and the gps-corrected wind vector (bottom). Solid lines: differences between *Polar2*- and *D-IBUF*-data.

4.3.4. Comparison of turbulence statistics.

The horizontal section of the flight can be used to compare turbulence measurements from the gust probes. For both aircraft the gps-correction is applied to the wind measurements. Prime quantities are computed by applying a high-pass filter with a cut-off frequency corresponding to a horizontal scale of 5 km. Since the available IBUF-data are sampled at 12.5 Hz, the Polar2 data for better comparison are also

used with 12.5 Hz sampling rate.

A comparison of heat and humidity flux measurements can not be made since the IBUF does not have fast sensors for temperature and humidity. Although the first order moments agree within a few percent of each other the comparison shows, that the higher order moments are very sensitive to measurements errors.

Table 5: Comparison of turbulence statistics. Listed are the standard deviations of the wind components σ_u , σ_v , σ_w , the mean wind speed \bar{U} , the friction velocity $u_* = (\overline{w'u'^2} + \overline{w'v'^2})^{0.25}$ and the drag coefficient $c_d = u_*^2/\bar{U}^2$.

	IBUF	Polar 2	difference
σ_u	2.60 m/s	2.67 m/s	2.6%
σ_v	2.43 m/s	2.51 m/s	3.2%
σ_w	0.63 m/s	0.68 m/s	7.6%
\bar{U}	7.88 m/s	8.05 m/s	2.1%
u_*	0.26 m/s	0.25 m/s	4.0%
c_d	$1.11 \cdot 10^3$	$0.96 \cdot 10^3$	14.5%

4.4. Dropsonde and aircraft intercomparison

On several days the flight patterns of *POLAR 4* were arranged such that an aircraft ascent from a height of 30 m above ground to 1800 m was followed by a dropsonde release and an aircraft descent again to a height of 30 m. The aircraft travelled a horizontal distance of about 20 km during an ascent or descent.

Figures 7 and 8 display dropsonde and aircraft data from intercomparisons. Since the dropsonde potential temperatures are between the aircraft sounding data, the differences presumably are due to horizontal temperature gradients. During some intercomparisons dropsondes overestimated temperatures by 1 to 2 K.

Relative humidities differ considerably. The dropsonde humidity data of more than 90 % (with respect to saturation over water) in the ground layer are reliable, since clouds have been observed there. The presence of ice particles in the clouds is probable, since the air temperatures are at -18°C . The aircraft humidity data, which are much lower than 85 %, do not reflect the cloud layer. The aircraft sensor shows a very slow response to the humidity causing a hysteresis effect between ascent and descent. The malfunction may be due to salt contamination.

The aircraft wind data slightly differ between the ascent and descent. Aircraft and dropsonde wind data are of the same magnitude, but dropsonde winds smooth wind variations away. The shear zone at the top of the inversion layer can be hardly detected from the dropsonde wind data. The radiosonde wind information based on the Ω -navigation system is less accurate than the aircraft INS and GPS positioning. The dropsonde wind calculation needs averaging over a large height interval to yield wind with an accuracy of ± 5 m/s, whereas the GPS-corrected wind has an instant accuracy of ± 0.25 m/s.

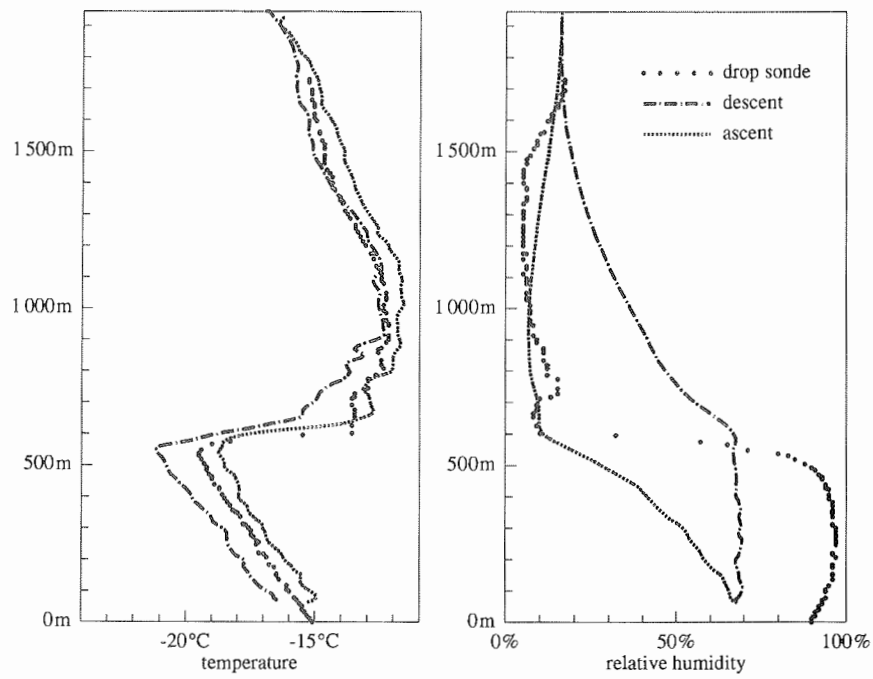


Figure 7: Comparison of temperature and relative humidity from aircraft ascent and descent and dropsonde data on March 23.

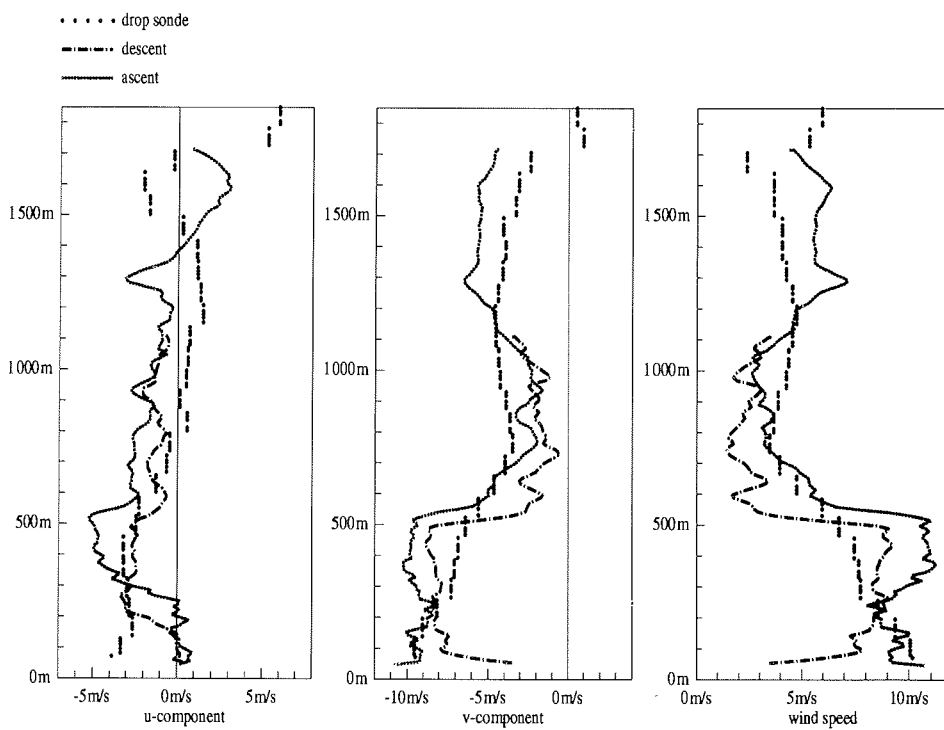


Figure 8: Intercomparison of wind speed and wind components from aircraft ascent and descent and dropsonde data on March 23.

5. Flight Catalogue

The following catalogue presents satellite images from NOAA satellites (channel 4) for the days of the experiment together with the ground tracks of either aircraft and three-dimensional views of flight paths. The satellite images are not precisely geocoded, the aircraft tracks are correct with respect to the latitude/longitude grid. Dropsonde releases are marked by circled black dots. Channel 4 data reflect ice surfaces and high clouds as white, low clouds as grey and water surfaces as dark.

Flights on February 28, 1993

The anticyclonic situation in the Spitzbergen region becomes weakened by a depression with altocumulus approaching from SW. The stratocumulus cloud deck over the ocean ends at the ice margin, no low clouds and only thin altostratus are present over the sea ice. North of 81.30°N thin ground fog is observed.

The *Polar 2* and *Polar 4* flights provide intercomparison data, checks on their instrumentation and in-flight calibrations. *Polar 2* also performs a northbound ice survey flight to 81.30°N. *Polar 4* inspects the landing strips of Ny Alesund and Svea.

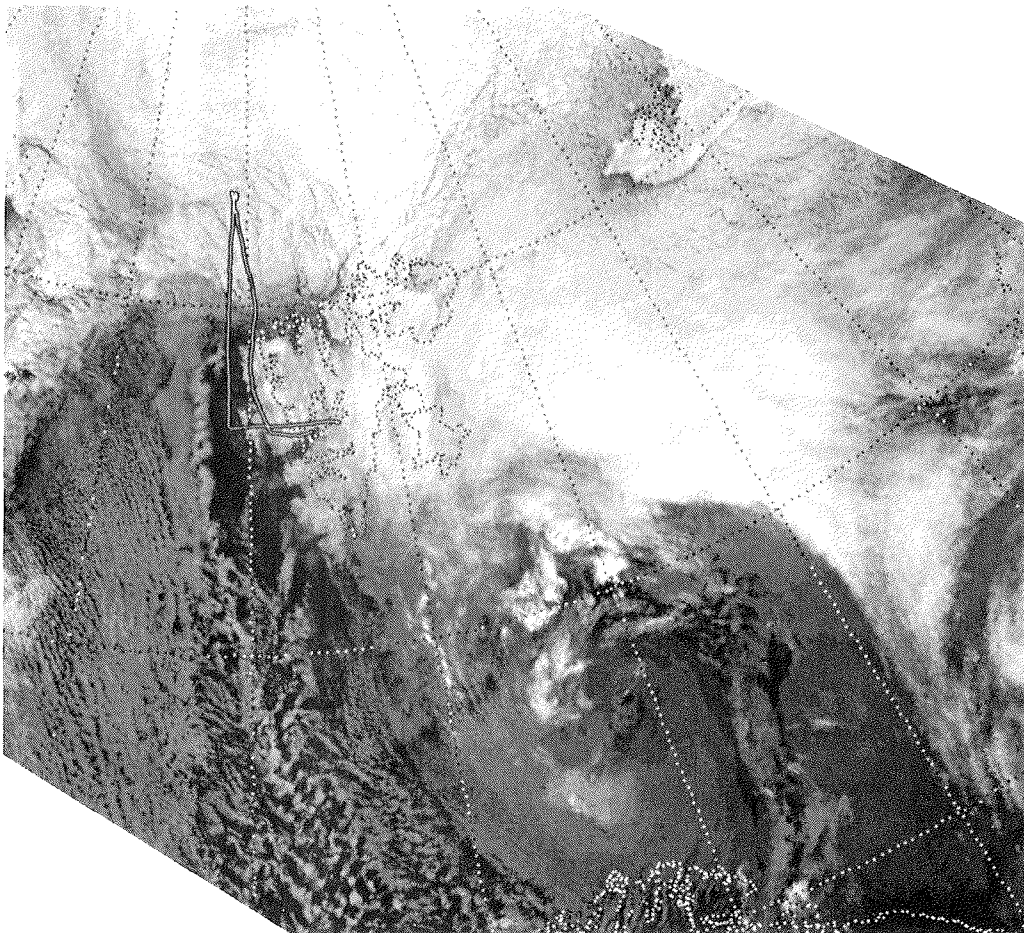
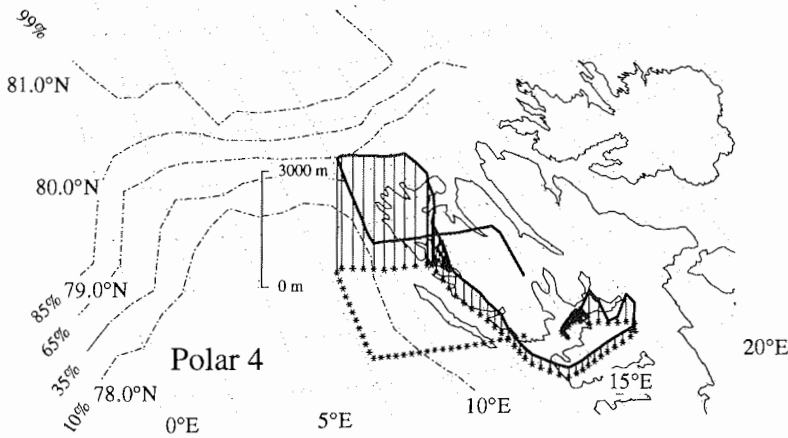
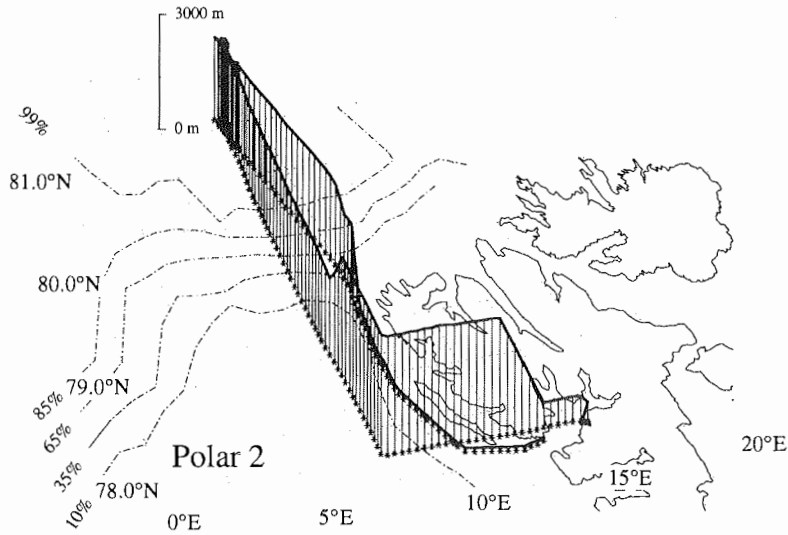


Figure 9: NOAA 11, 04:47:00, Polar 2 flight track.

28 February 1993



Flights on March 4, 1993

On the rear side of depressions southeast of Spitzbergen a cold air mass passes the marginal ice zone from the north. No clouds are observed in the sea ice region and over Spitzbergen. Leads cause the development of sea fog near the ice margin, which becomes more intense over the ocean. The oceanic region is covered by 6-7/8 of stratocumulus.

Polar 2 first performs a westbound ascent and intercomparison flight with the D-IBUF, then turns northward for linescan observations at FL 100 to 81°N and performs low level traverses across the ice margin (80.30°N) and at 78.30°N. *Polar 4* turns to the west from Longyearbyen and during a northbound flight 9 dropsondes are released from the aircraft to document the air mass transformation during the cold air outbreak.

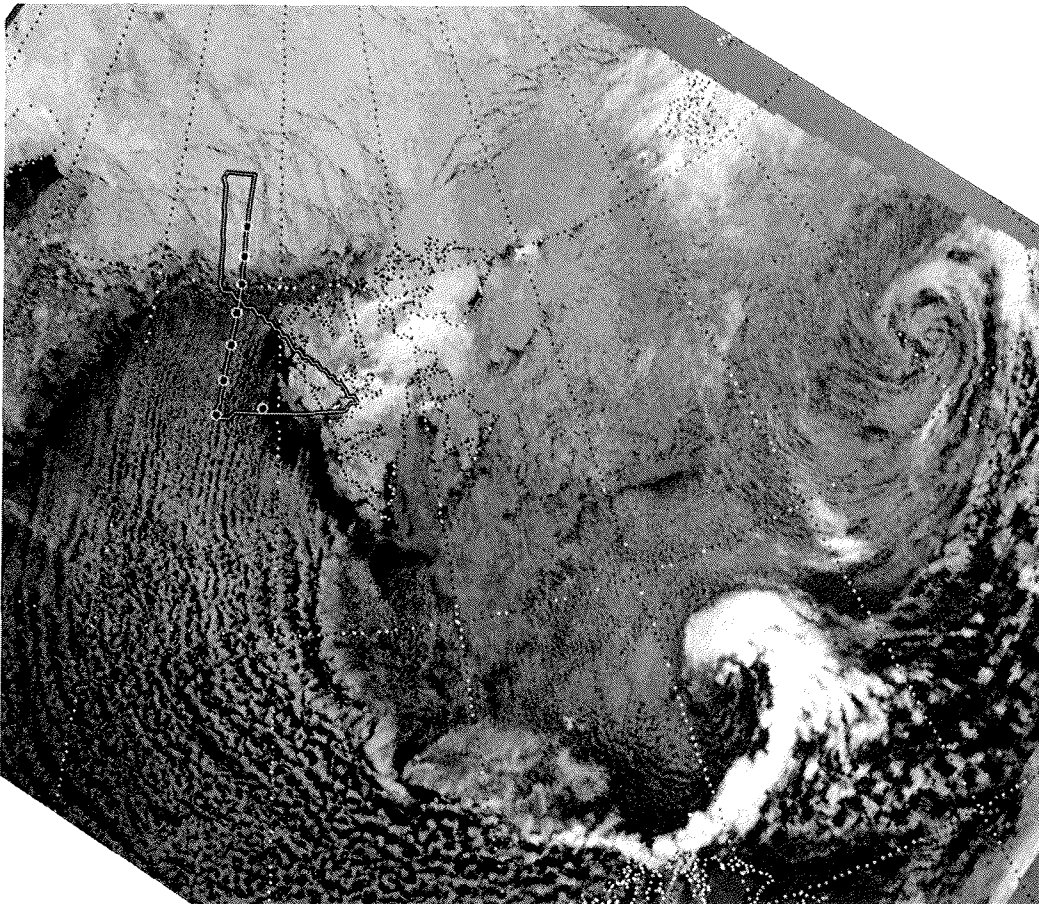
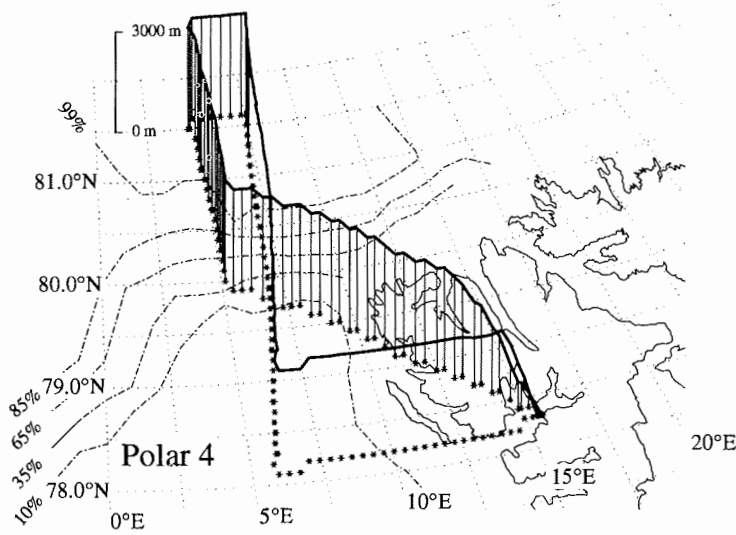
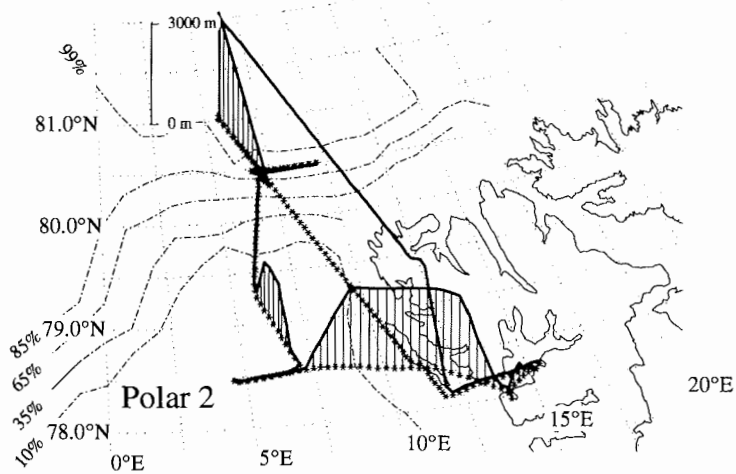


Figure 10: NOAA 12, 08:42:00, Polar 4 flight track.

04 March 1993



Flights on March 5, 1993

The situation is similar to the previous day with anticyclonic conditions and a northerly flow. No clouds are present over the sea ice region but 6-8/8 Sc over the ocean.

The two aircraft meet to the west of Spitzbergen and perform an intercomparison and LSC northbound flight in loose combination to 80.30°N. Superposed flights at different levels are performed to study atmospheric radiational effects. *Polar 2* and *Polar 4* then pass the *POLARSTERN* position towards the ice margin for turbulence studies and intercomparisons.

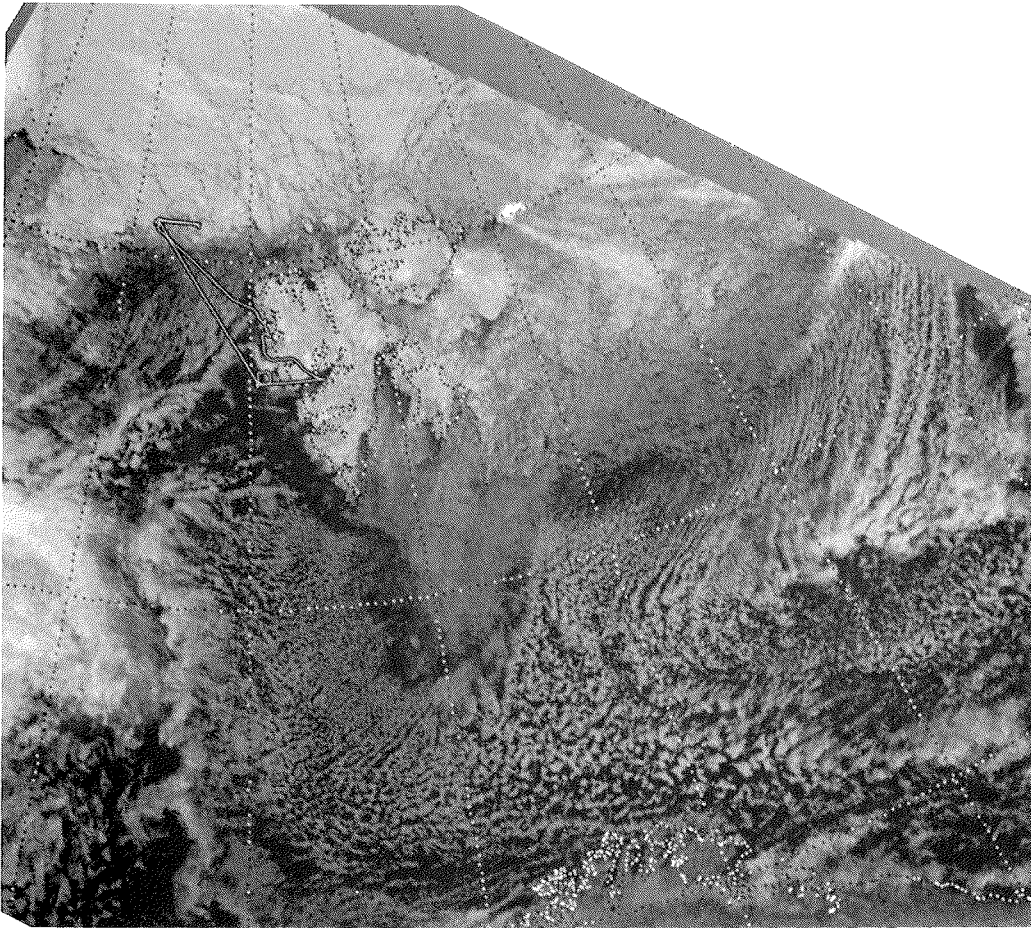
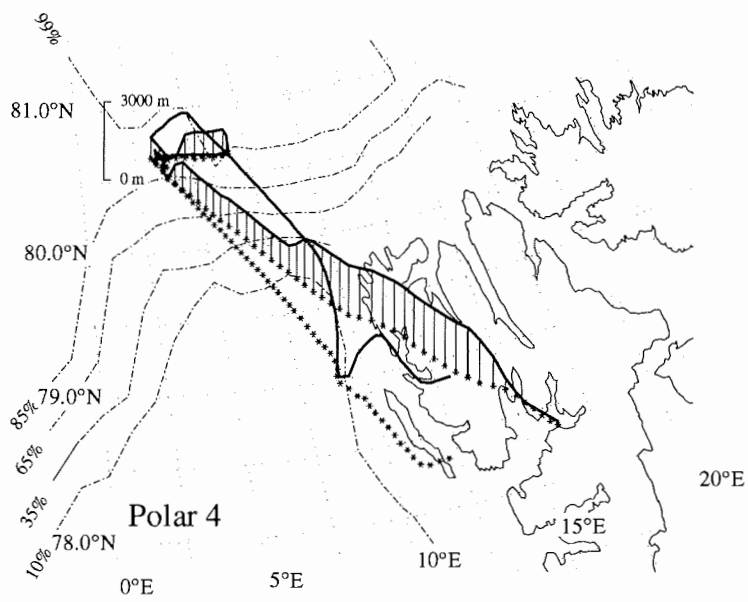
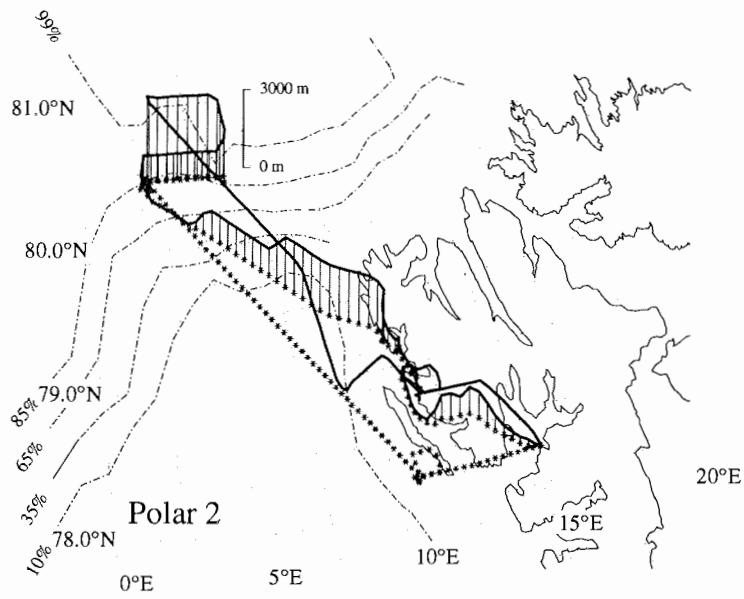


Figure 11: NOAA 12, 08:21:00, Polar 4 flight track.

05 March 1993



Flights on March 10, 1993

A weak outbreak of cold air determines the weather conditions in the Spitzbergen region. No clouds are present north of 80.40°N. Sea fog develops over leads and open water at the ice margin. 6/8 cumulus clouds over the ocean have a distinct roll-type appearance.

Polar 2 performs a northbound flight at FL 60 over *Polarstern* at position 81.25°N, 6.5°E. The return flight to the ice margin at 100 ft and 4 superposed flight legs provide turbulence, laser altimeter and linescan camera data.

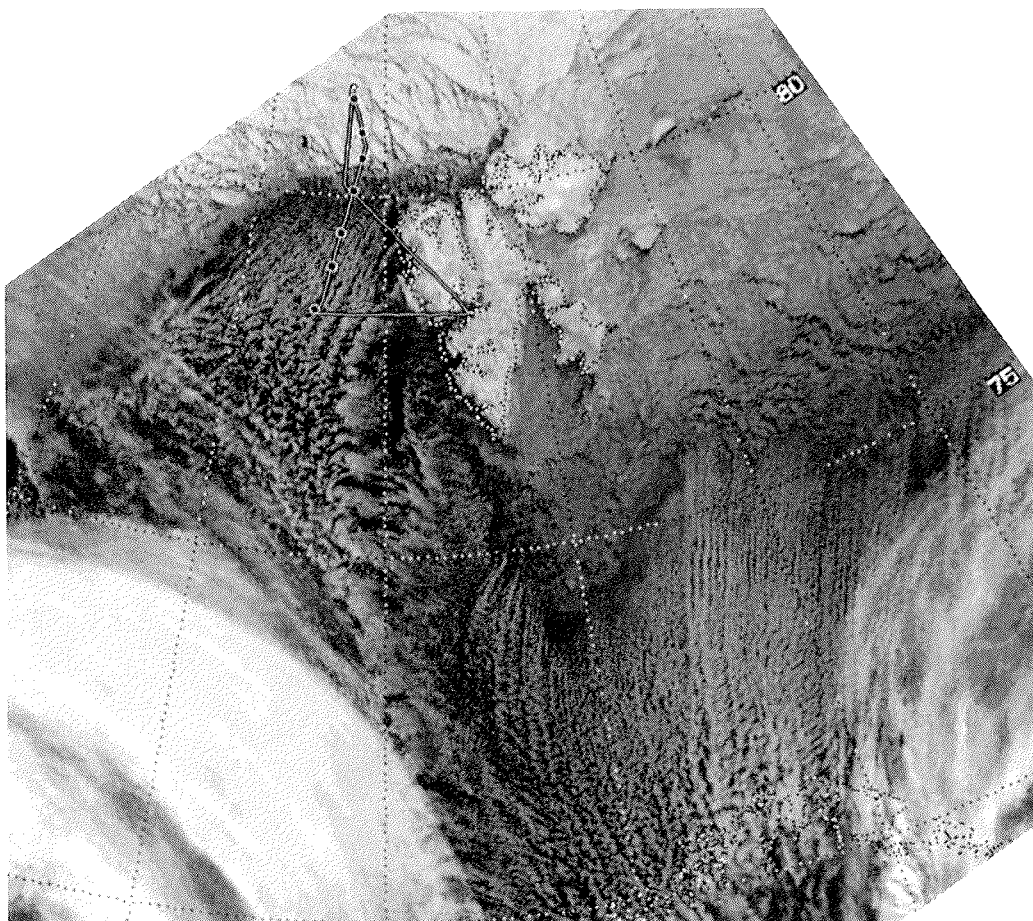
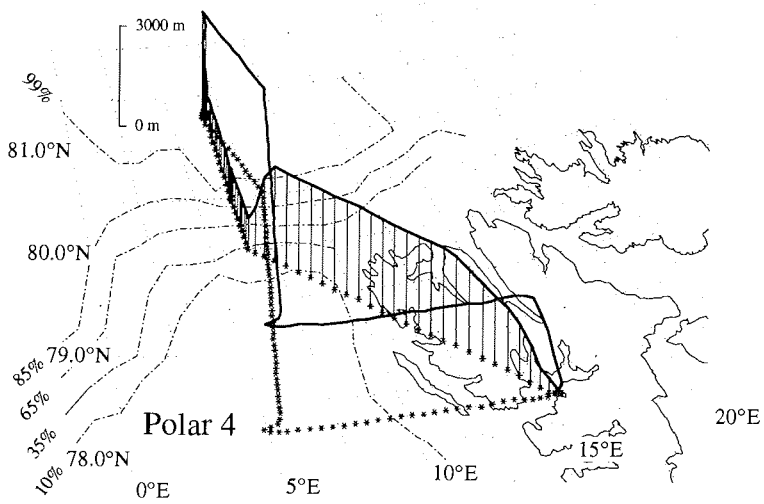
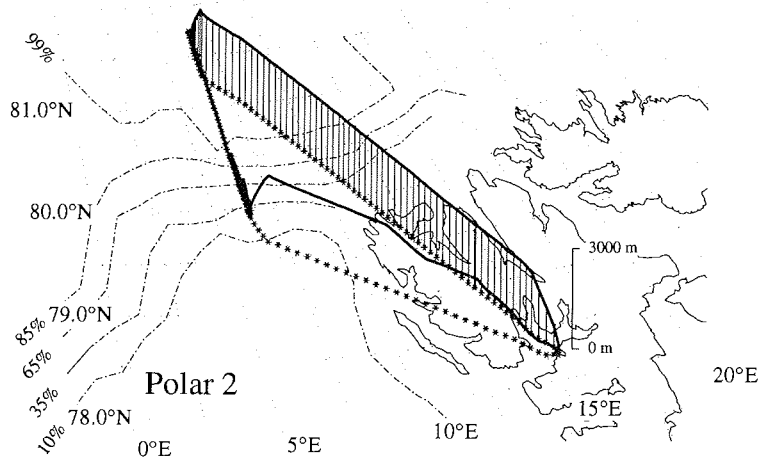


Figure 12: NOAA 11, 12:49:16, Polar 4 flight track.

10 March 1993



Flights on March 11, 1993

The high pressure situation with weak pressure gradients persists. Winds are northerly. No high clouds, but shallow fog and haze - thickening towards the ice edge - is observed in the sea ice zone. The ocean is covered by 6-8/8 Sc.

The aircraft carry out a comparison with the BSRN-station at Ny Alesund. *Polar 4* then performs a northbound flight with a series of drop-soundings to the position of *Polarstern*. The *Polar 2*-flights at heights of FL 100 resp. 100 ft over the *Polarstern*-position provide LSC-, IRLS- and turbulence data. Low level flight legs near the ice edge are repeated 4 times for turbulence studies.

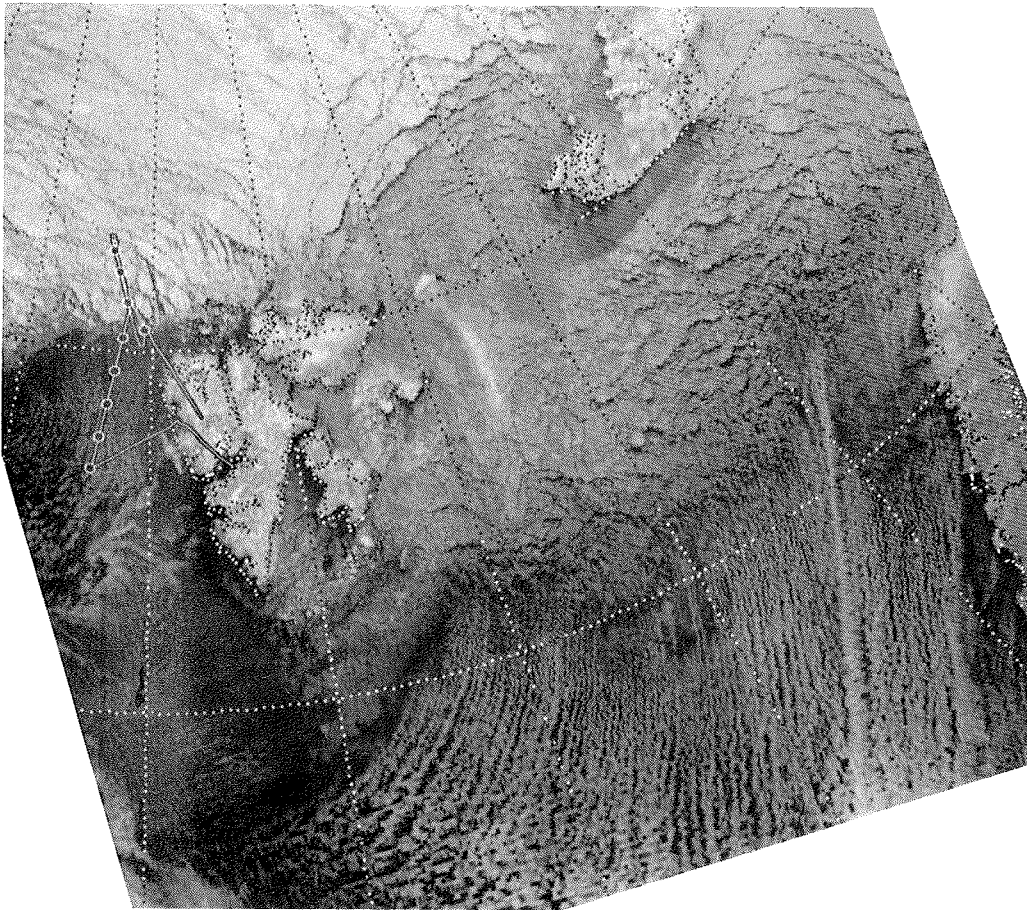
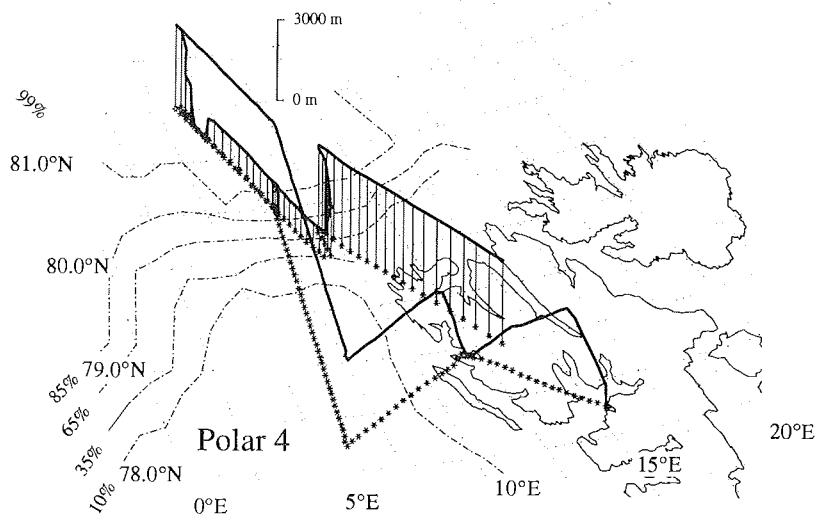
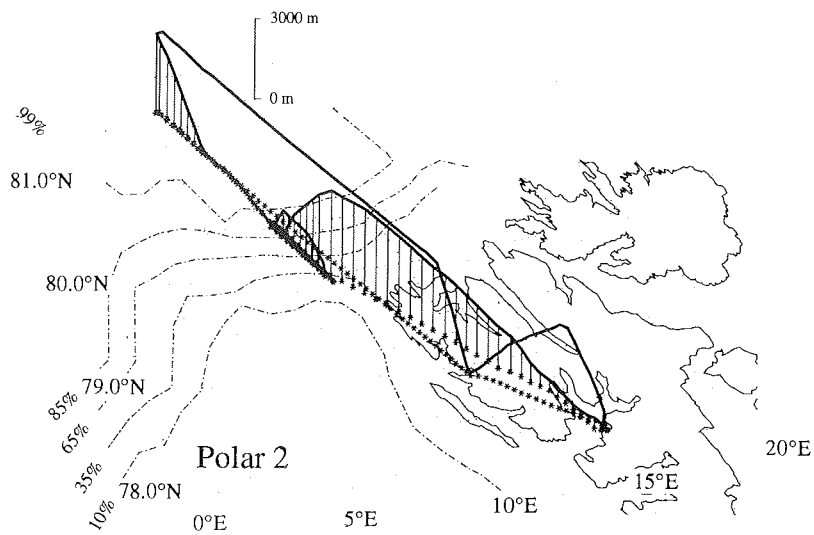


Figure 13: NOAA 11, 07:35:00 , Polar 4 flight track.

11 March 1993



Flights on March 12, 1993

The ridge of an anticyclone over Northern Greenland extends over Spitzbergen. To the west of Spitzbergen a depression with midlevel and high clouds gradually moves northward. Winds are weak and variable in the sea ice zone, where visibilities are reduced by haze.

Polar 2 performs a LSC- and IRLS-flight over the position of *Polarstern* to 81.25°N. During the low-level return flight the vessel is passed again for turbulence and radiation intercomparisons. During further flight legs at 100 ft north of the ice margin turbulence and laser data are obtained.

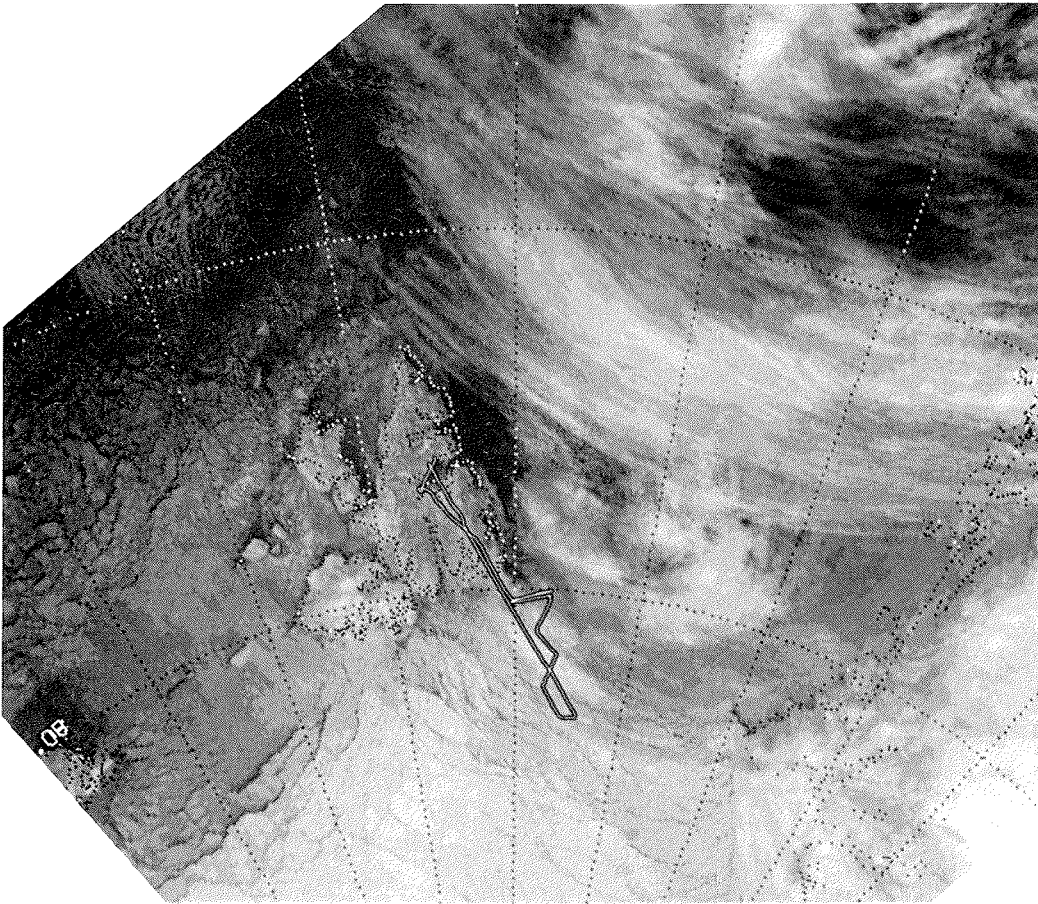
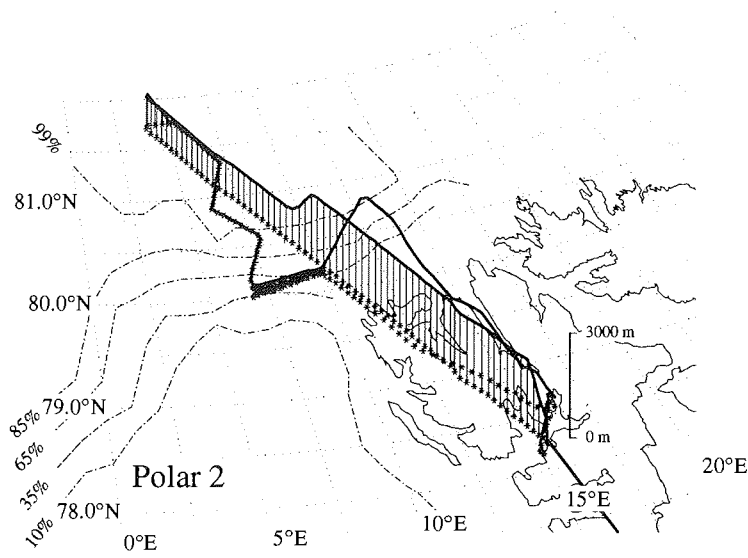


Figure 14: NOAA 11, 12:26:13, Polar 2 flight track.

12 March 1993



Flights on March 16, 1993

Small pressure differences cause weak winds from the north. Stratus clouds are present in the sea ice zone south of the position of *Polarstern* (80.8°N). They become broken north of 81°N. Thick sea fog develops over open water at the ice margin.

At heights of 100 ft above ground (*Polar 2*) and 1000 ft above cloud tops (*Polar 4*) the aircraft pass the *Polarstern* position towards 81.4°N to obtain turbulence data and to detect cloud radiational effects. Simultaneous superposed flight legs are repeatedly flown by the aircraft near the ice edge for the same purpose.

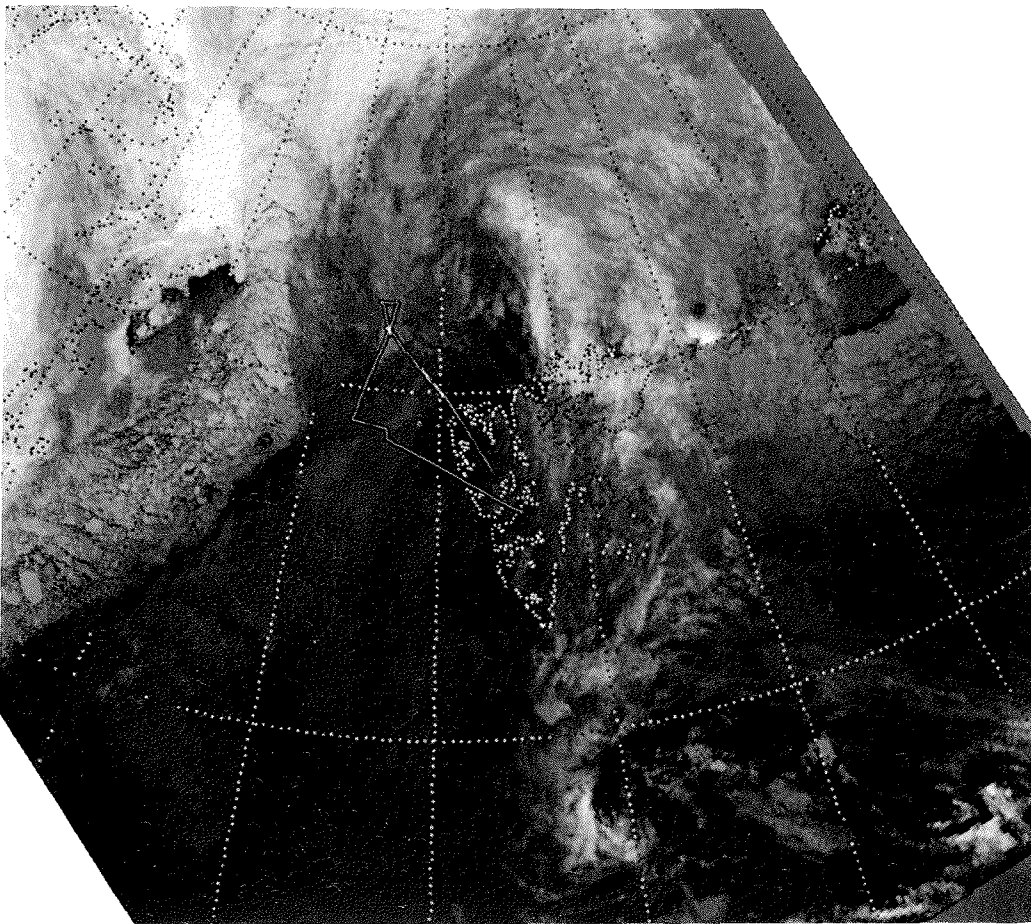
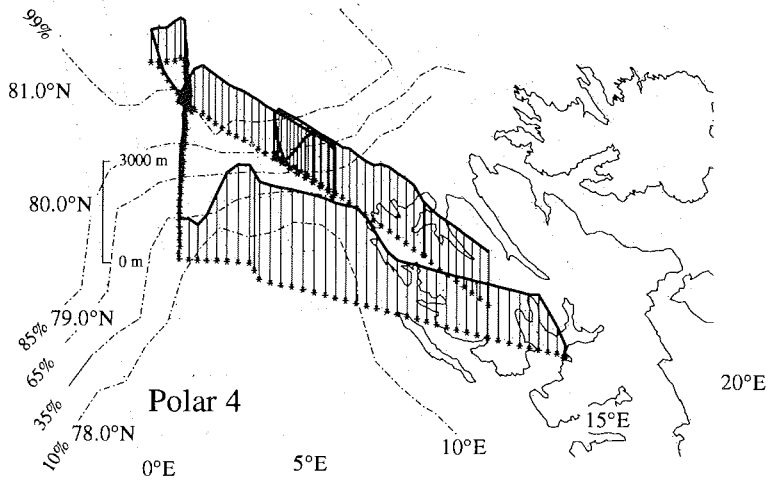
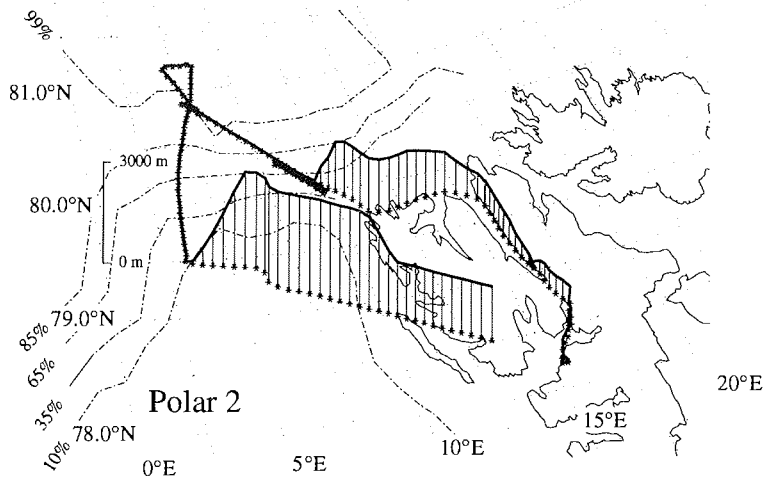


Figure 15: NOAA 10, 09:21:00, Polar 4 flight track.

16 March 1993



Flights on March 17, 1993

A weak low-pressure system is situated north of Spitzbergen. A tongue of moist air extends to the south from the center of the depression and over Spitzbergen. Cloud tops within the moist zone are at 2300 m. Pressure gradients in the sea ice zone west of 10 °E are weak. No high or midlevel clouds are observed there. Strong sea fog develops from the leads and changes to stratocumulus over the ocean west of Spitzbergen.

Polar 2 performs a high-level LSC- and IRLS-ice-survey to the position of *Polarstern*. The vessel is then passed three times at a height of 100 ft for turbulence studies and sensor intercomparison. Flight legs at 100 ft for turbulence studies are flown seven times near the ice edge.

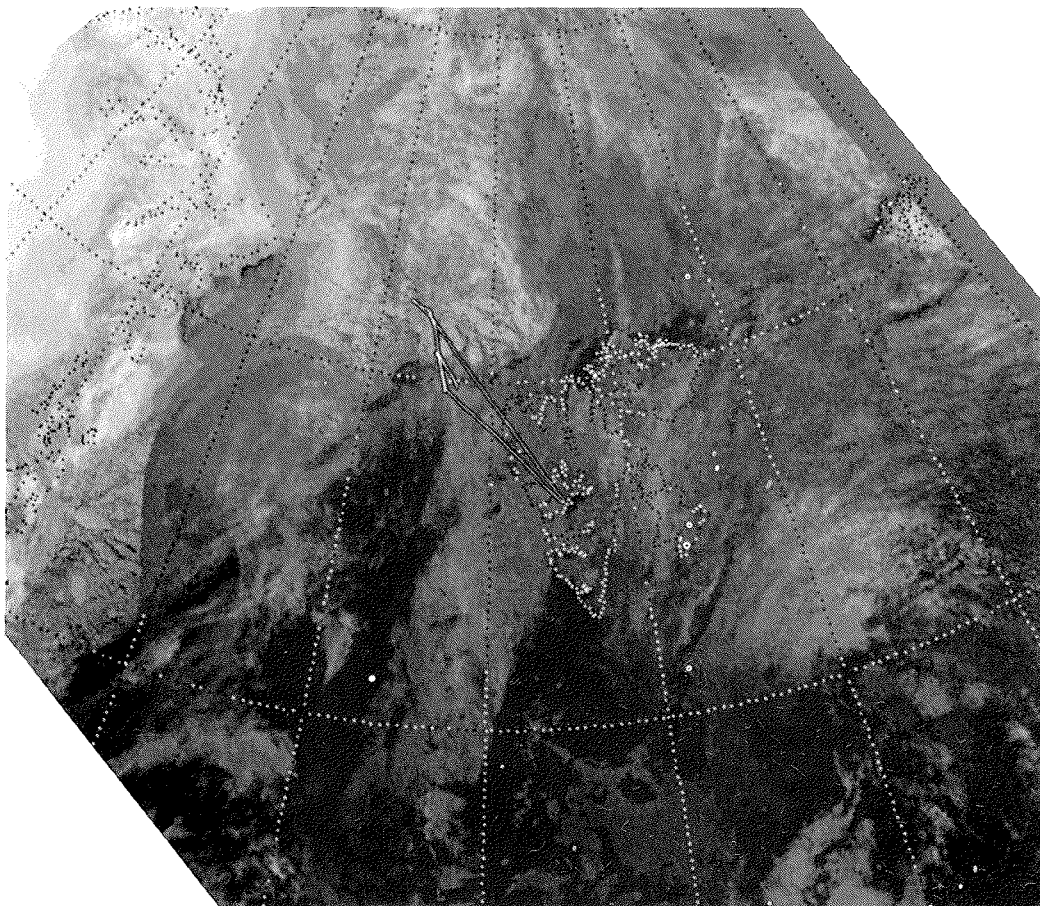
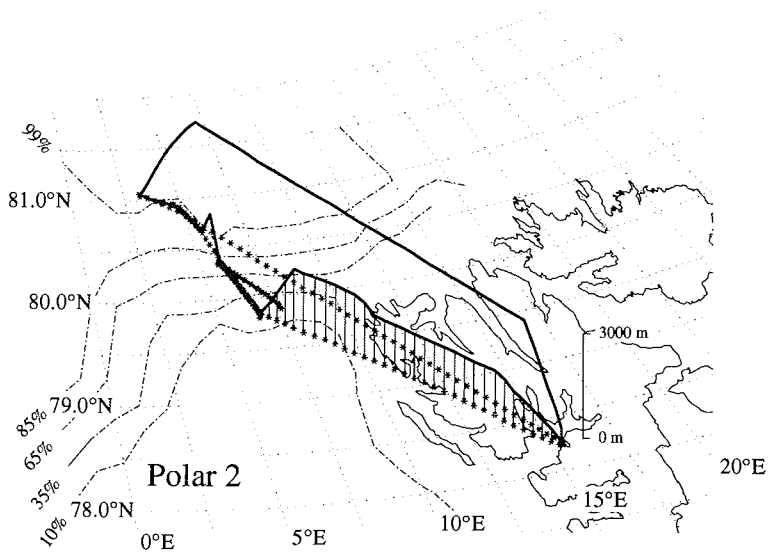


Figure 16: NOAA 10, 08:57:00, Polar 2 flight track.

17 March 1993



Flights on March 19, 1993

Cold air is advected with a northerly flow in the boundary layer, while a southeasterly flow persists above. The oceanic region west of Spitzbergen is covered with 8/8 Sc. Cloud conditions are variable in the sea ice zone. The bases of the Sc are between 300 ft and 600 ft, the tops are between 2000 ft and 5000 ft.

Polar 2 and *Polar 4* obtain meteorological fields with high resolution within a box of 100 km horizontal extent over the ice margin. *Polar 2* measures turbulent fluxes and the radiation balance near the surface, while *Polar 4* performs multiple ascents and descents as well as dropsoundings. Dropsondes are also released downstream of the box. *Polar 2* obtains LSC- and ILRS-data during a high-level over *Polarstern* and airborne data comparison data during three low level passes of the vessel.

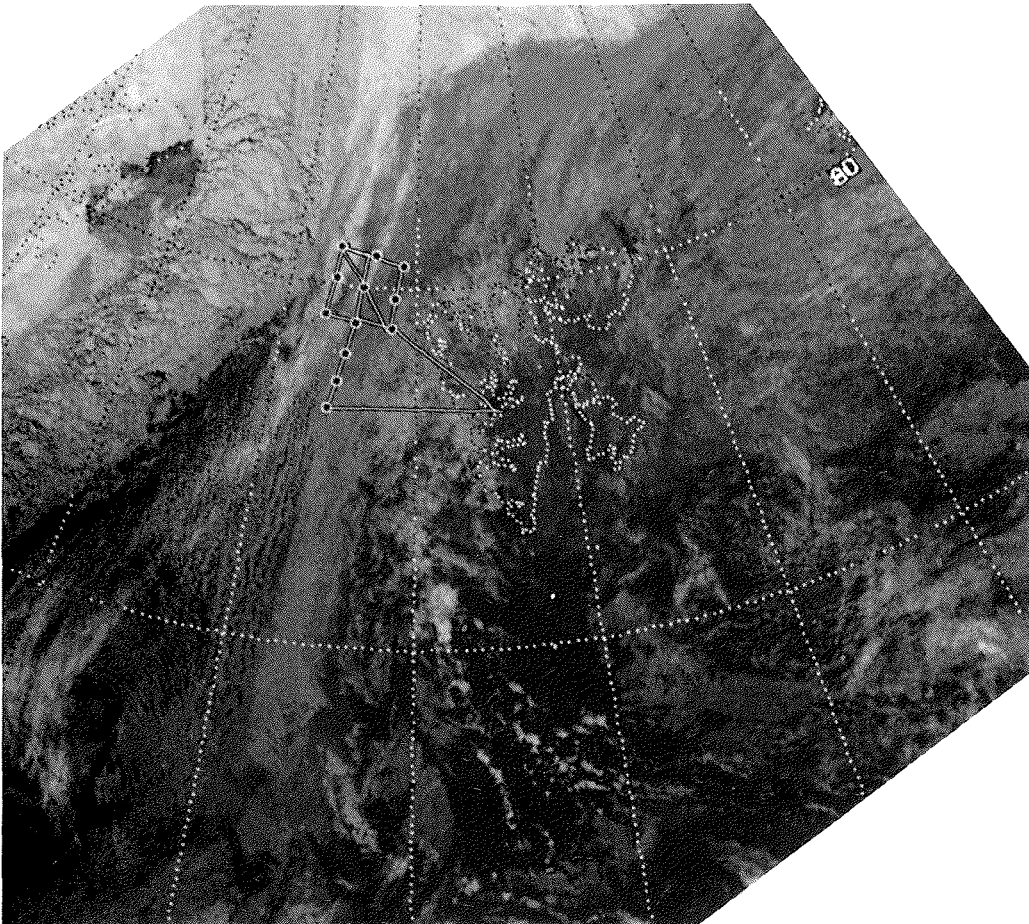


Figure 17: NOAA 11, 12:41:24, Polar 4 flight track.

Flights on March 20, 1993

Rising pressure over Greenland causes the development of anticyclonic conditions to the west and northwest of Spitzbergen. The cold-air outbreak with a northerly flow becomes weaker in the course of the day and winds change to easterlies in the marginal ice zone.

Similar to the day before, the flights of *Polar 2* and *Polar 4* are coordinated to obtain meteorological fields with a high resolution within a box of 100 km horizontal extent and 2 km vertical extent over the ice margin. *Polar 2* obtains turbulent fluxes and the radiation balance near the surface, while *Polar 4* performs multiple ascents and descents as well as dropsoundings on the periphery of the box. Dropsondes are also released along the air mass trajectory south of the box.

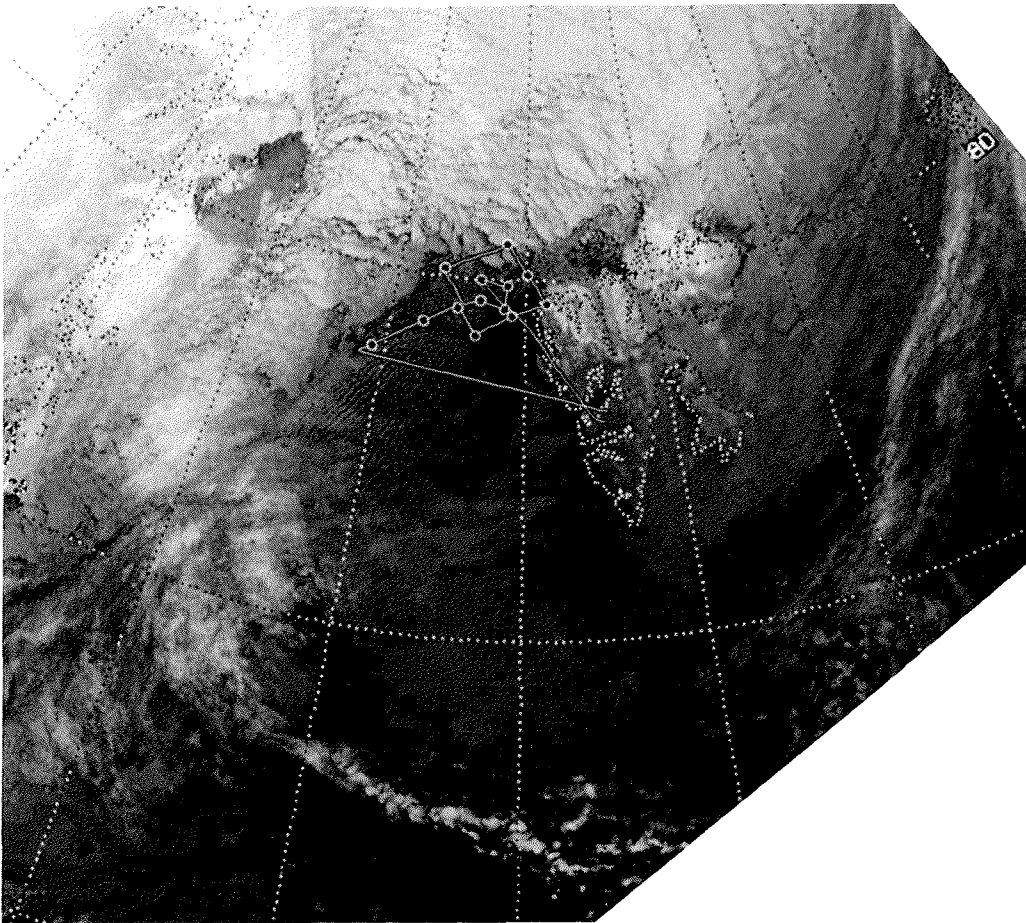
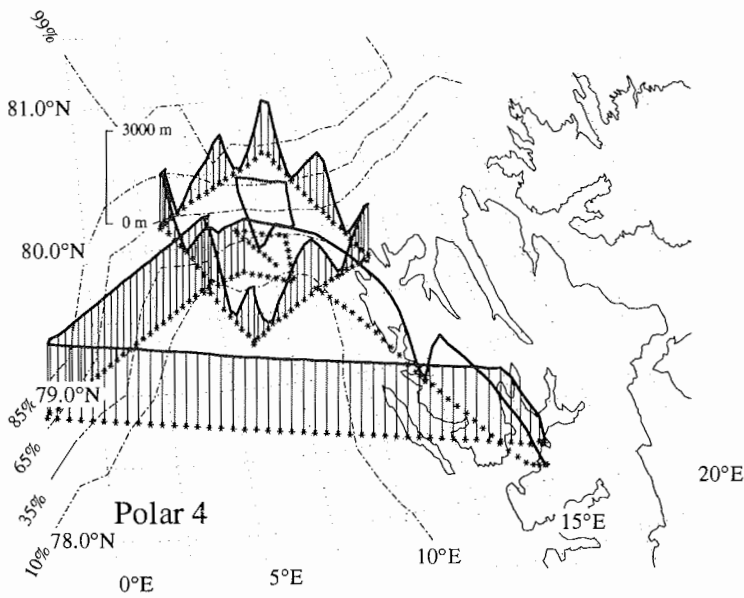
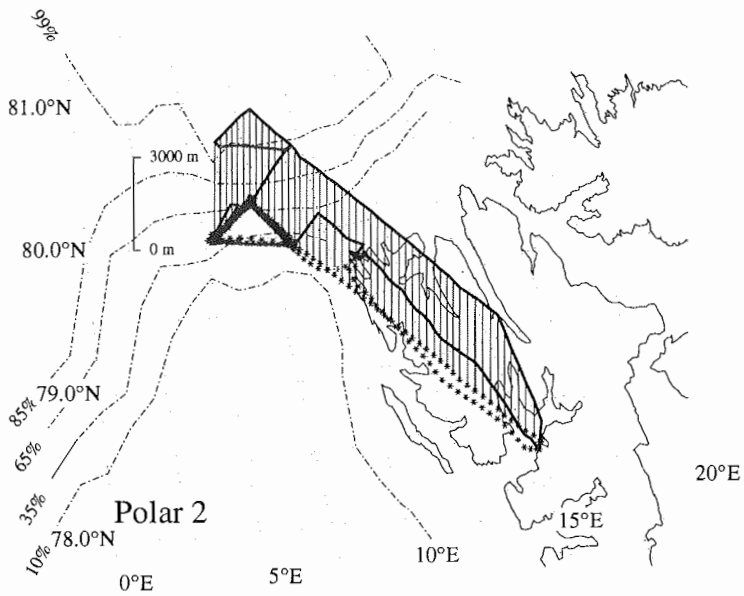


Figure 18: NOAA 11, 12:29:44, Polar 4 flight track.

20 March 1993



Flights on March 23, 1993

Anticyclonic conditions with a weak pressure distribution cause moderate wind speeds. The sea ice is covered with extended haze fields. Intense sea fog develops over leads and south of the ice margin. 7/8 Sc is observed over the ocean.

The aircraft are used for a similar mission to the previous days. They obtain meteorological fields with a high resolution within a box of 100 km horizontal extent and 2 km vertical extent over the ice margin. *Polar 2* measure turbulent fluxes and the radiation balance near the surface, while *Polar 4* performs multiple ascents and descents as well as dropsoundings on the periphery of the box.

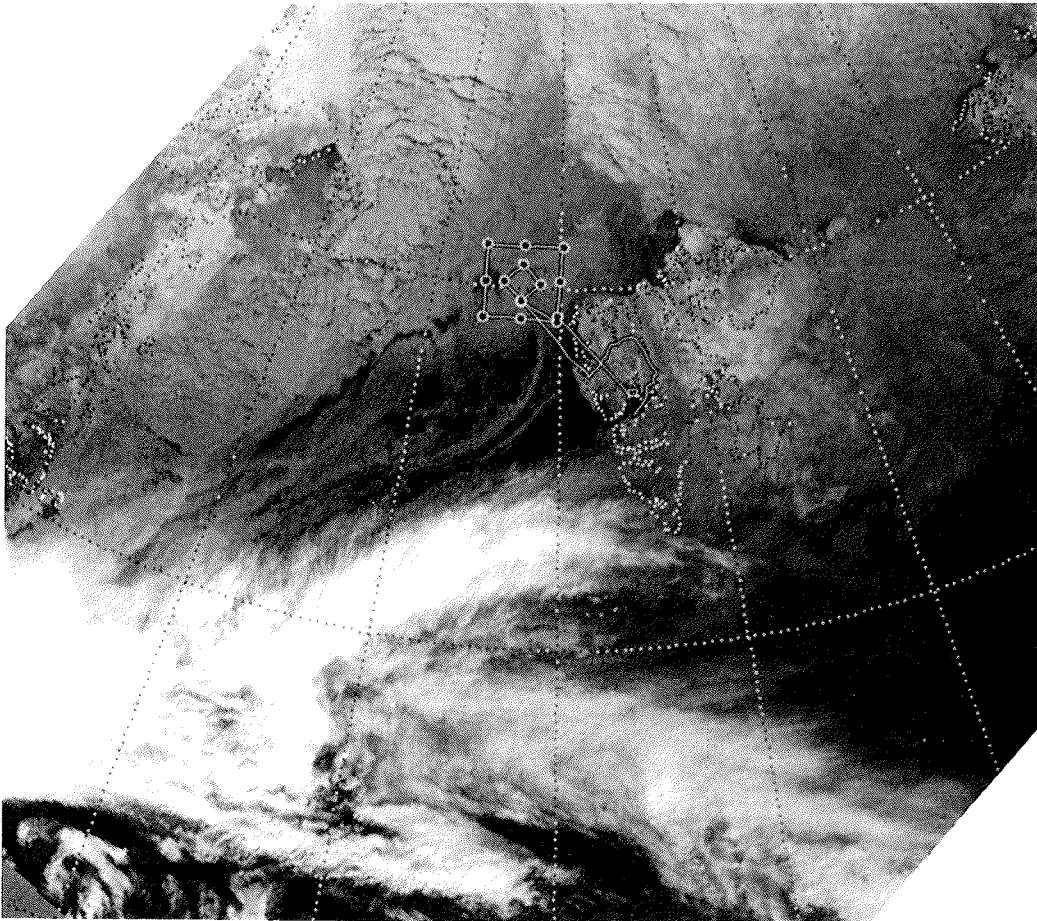
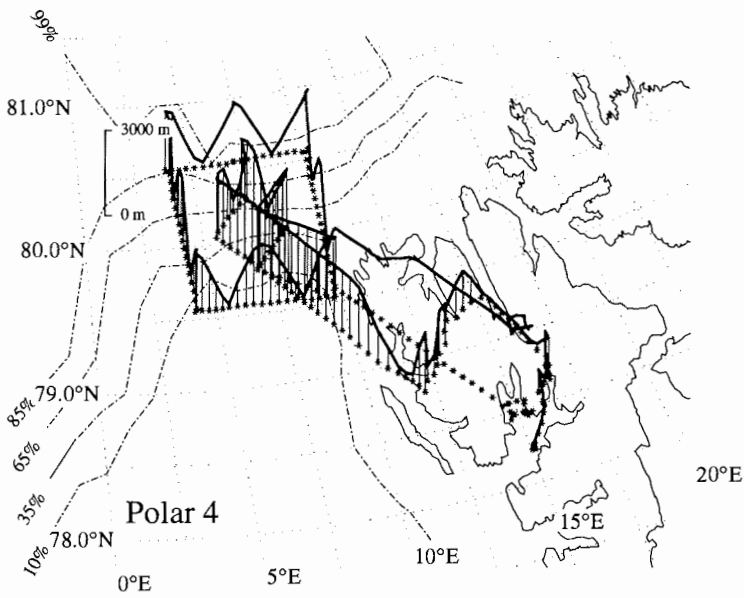
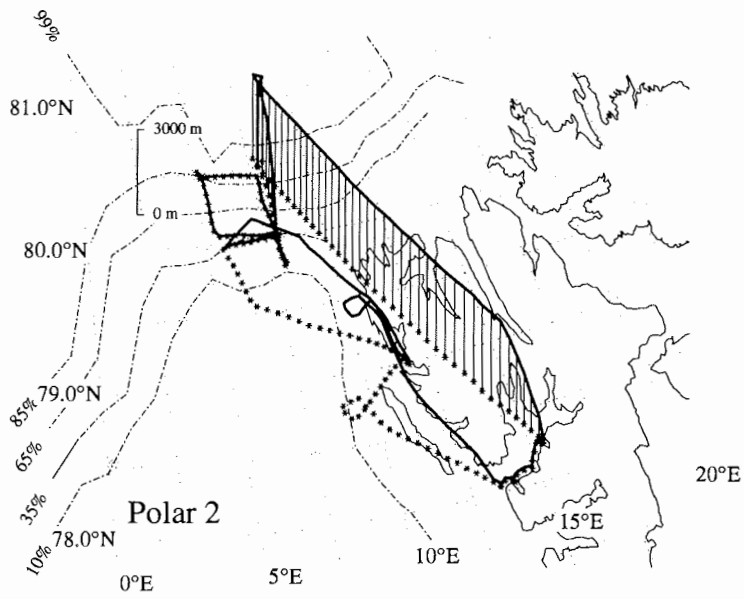


Figure 19: NOAA 11, 11:52:45, Polar 4 flight track.

23 March 1993



Flights on March 25, 1993

A low pressure system passes Spitzbergen on a route remaining south of the archipelago. In the marginal ice zone anticyclonic conditions persist.

The aircraft perform missions similar to the three previous days. They obtain near surface fluxes (*Polar 2*) and profiles of humidity, temperature, wind and radiation by aircraft ascents and descents as well as by radiosonde drops (*Polar 4*).

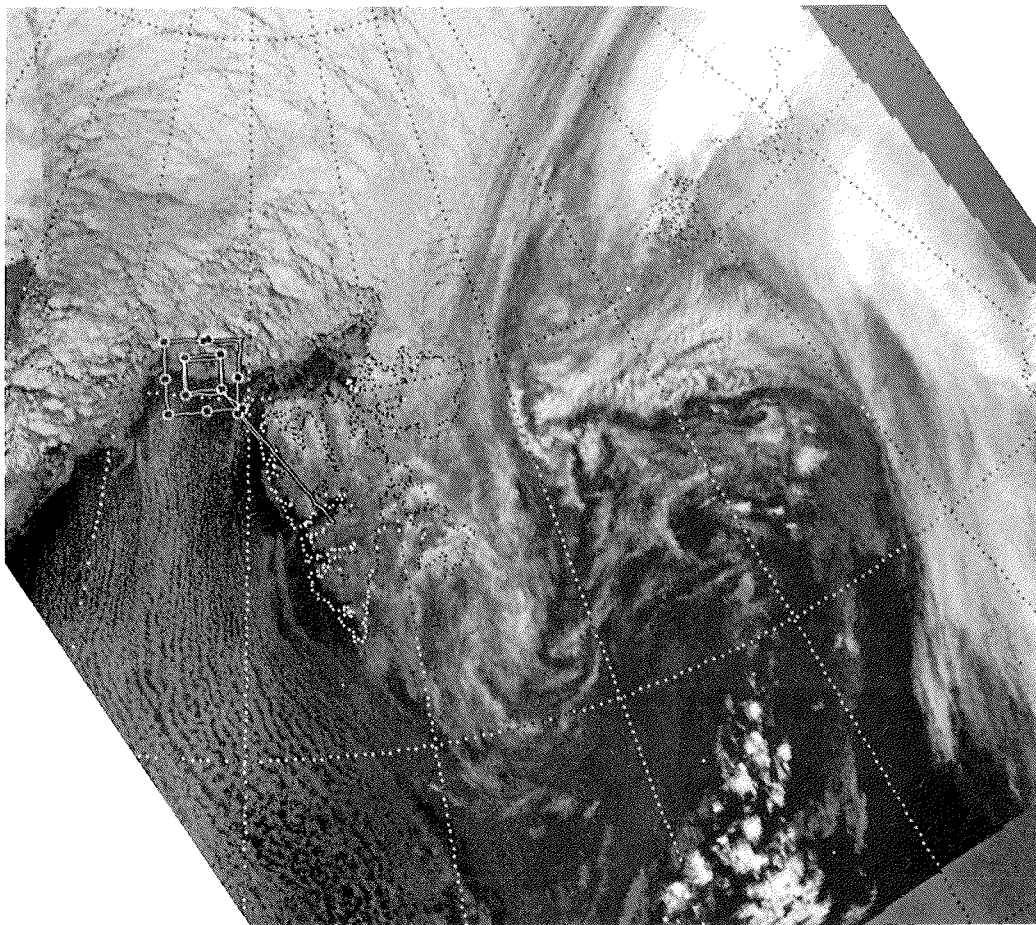
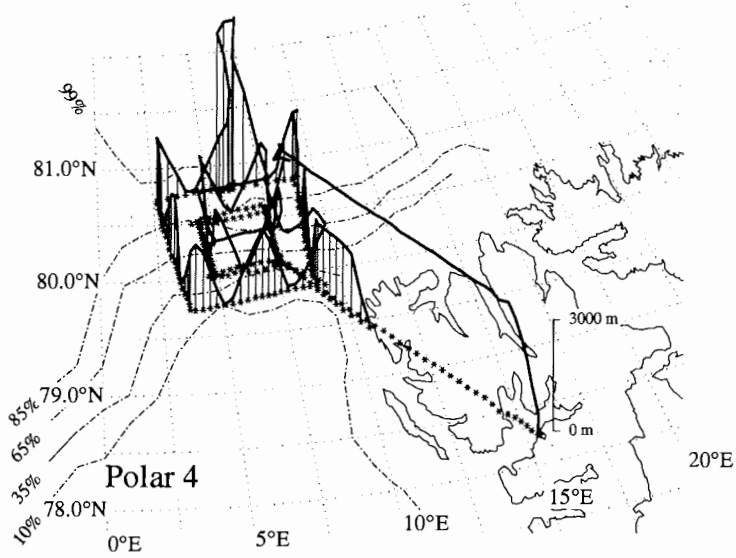
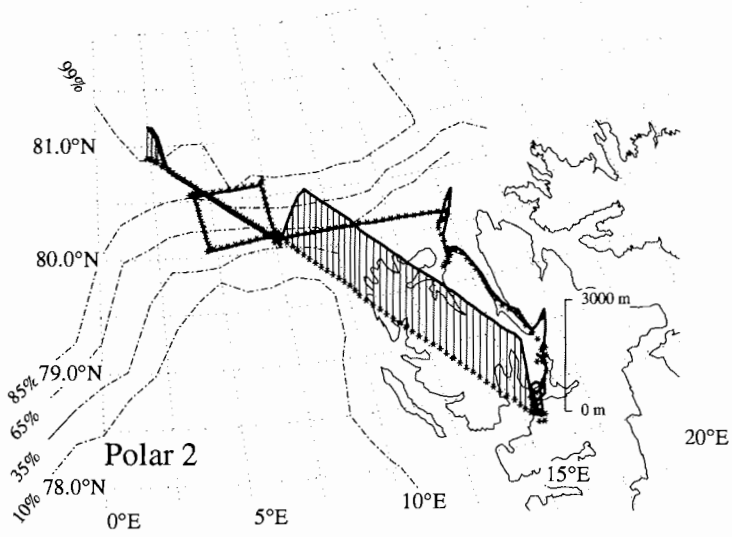


Figure 20: NOAA 11, 06:26:00, Polar 4 flight track.

25 March 1993



6. Data Presentation

In this section a few examples of typical features measured during the experiment are presented. This is meant to illustrate the obtained data set and its adequacy for further analyses to meet the scientific objectives of REFLEX II.

6.1. Detection of surface structure by laser altimeter measurements

The height of the aircraft above the local sea level must be known with an accuracy of ≈ 2 cm to compute the surface profile from the distance measurement of the laser altimeter. The high frequency vertical movement can be derived from the aircraft's inertial system (INS). The accuracy of the vertical acceleration measurement is sufficient to allow an integration over up to a minute, corresponding to 5 km distance at normal speed.

Scales beyond this 5 km cannot be resolved, as none of the other height measurements can provide sufficient accuracy: The selected-availability code of **GPS** imposes errors of $\sigma_z = 60$ m on the vertical component of the position. The spectrum of these fluctuations peaks around a period of 600 s. Averaging over about one minute, the time to fly 5 km, therefore does not reduce this error to anywhere near the required 2 cm. The **radar altimeter** measures the height above the local sea level only over open water. Over ice the echo is a complex mixture of reflections from inside the ice floes, leading to an apparent increased distance over thick ice. The **static air pressure** typically varies by 1 hpa over 100 km on the synoptic scale. Near sea level this corresponds to some 50 cm height difference over 5 km distance. The resulting error is 25 times too large for a correct height reference.

The recorded signal is subjected to a filter that removes white noise with a standard deviation of 0.03 m, a value found by recording the laser altimeter pointing at a white surface at 30 m distance. Three consecutive samples are then averaged, reducing the distance between samples to the diameter of the beam at 30 m. The surface height profile is then calculated as the difference between the high-pass filtered height of the aircraft (from INS integration) and the high-pass filtered laser distance. Lastly, from each surface point the minimum in the vicinity of 2.5 km is subtracted.

Figure 21 shows an example of the laser profile from a flight in closed pack ice with ridged floes and leads covered by nilas. Also shown is the surface temperature measured by the KT4 radiation thermometer.

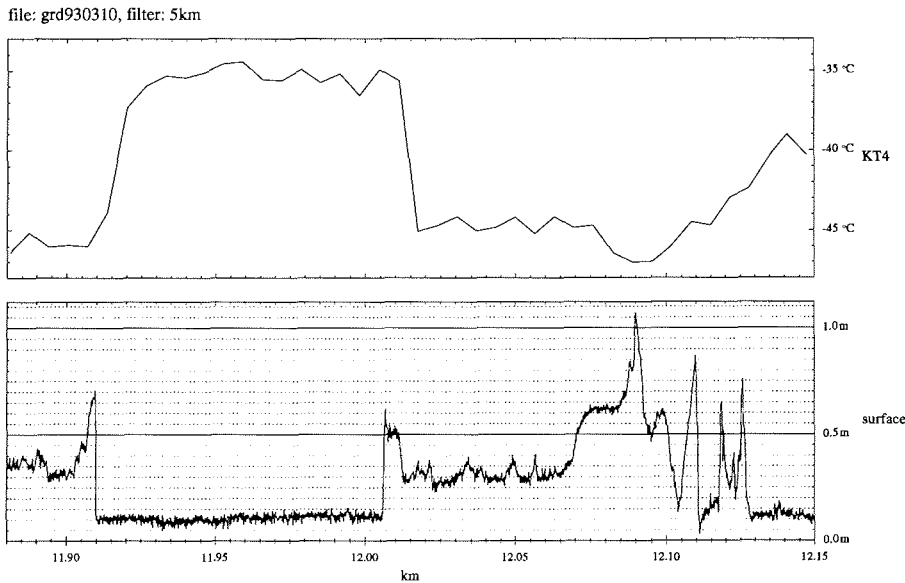


Figure 21: An example of laseraltimeter and KT4-data

6.2. Observations with the Line Scanner Systems

The digital images are geometrically adjusted, the infrared line scanner (IRLS) data are temperature calibrated and erroneous scans are eliminated. Then images of the visible and infrared bands are produced. The data are processed to derive different ice parameters. Figure 22 shows an example of the ice, nilas (new ice), water and temperature distribution, observed during a flight at an altitude of about 2 km over the marginal ice zone on 28 Feb 28, 1993. Both images cover an area of about 20 km^2 ($4 \times 5 \text{ km}$). Similar data were acquired during 11 flights, covering a total area of more than 3000 km^2 .

The upper figure displays the *LSC*-data, where dark, gray and light areas correspond to water, nilas and snow covered ice fields, respectively. The surface temperatures obtained by the *IRLS* (bottom) range between $-2 \text{ }^\circ\text{C}$ (black) and $-27 \text{ }^\circ\text{C}$ (white). Typical surface features are reflected by both figures, i.e. ice free cracks and leads, new ice fields and snow covered ice floes of different sizes. The bulk ice structures are similarly discriminated by both systems. The *IRLS* resolves many details much better than the *LSC*, since the shortwave reflectivity of snow covered ice floes hardly depends on the thickness and structure of the ice floes. Different ice thicknesses,

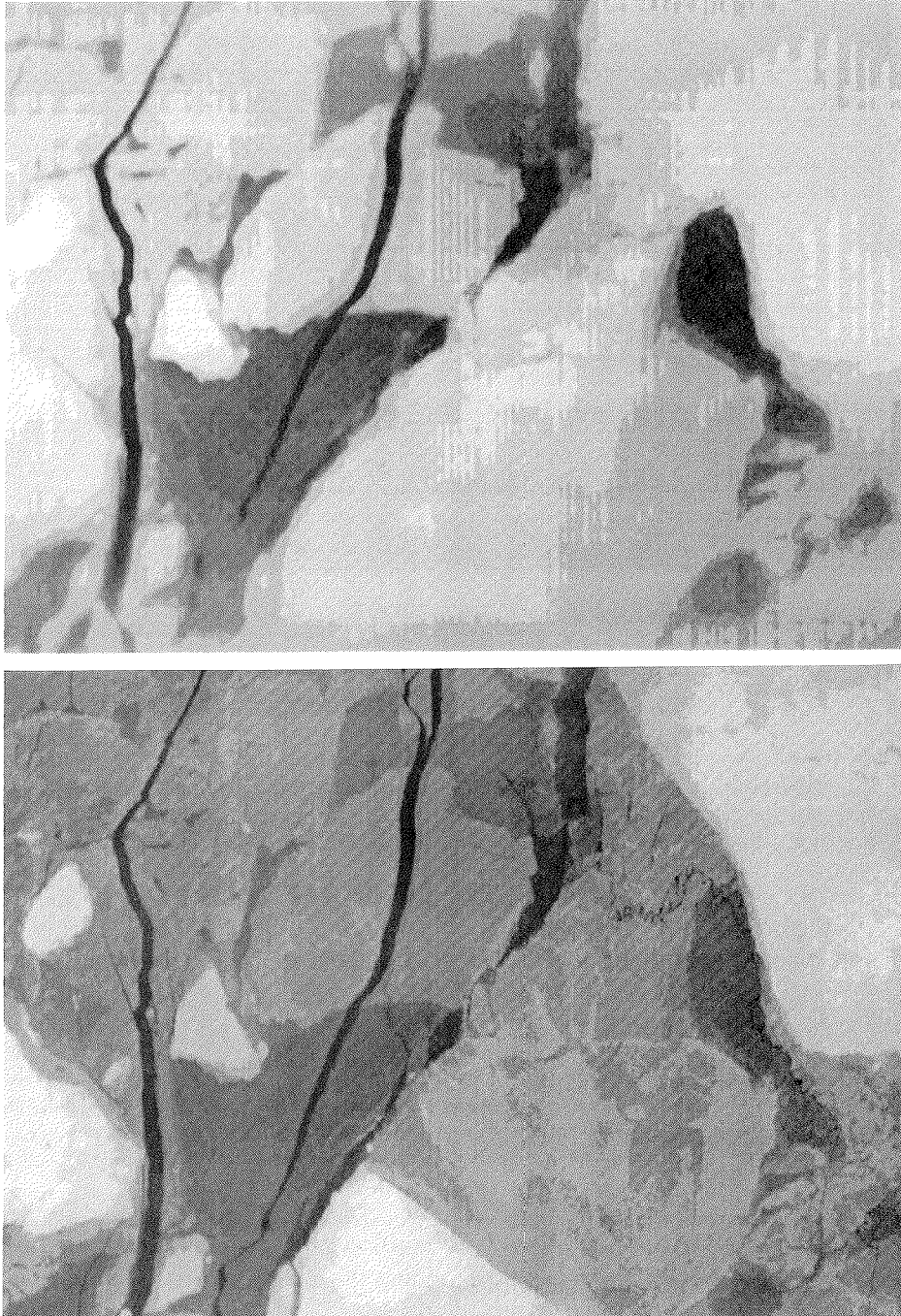


Figure 22: Shortwave reflectivity (*LSC* top) and surface temperature (*IRLS* bottom) obtained for a 4 x 5 km scene 50 km to the north of the ice margin. Surface temperatures span the range from -27°C (white) to -2°C .

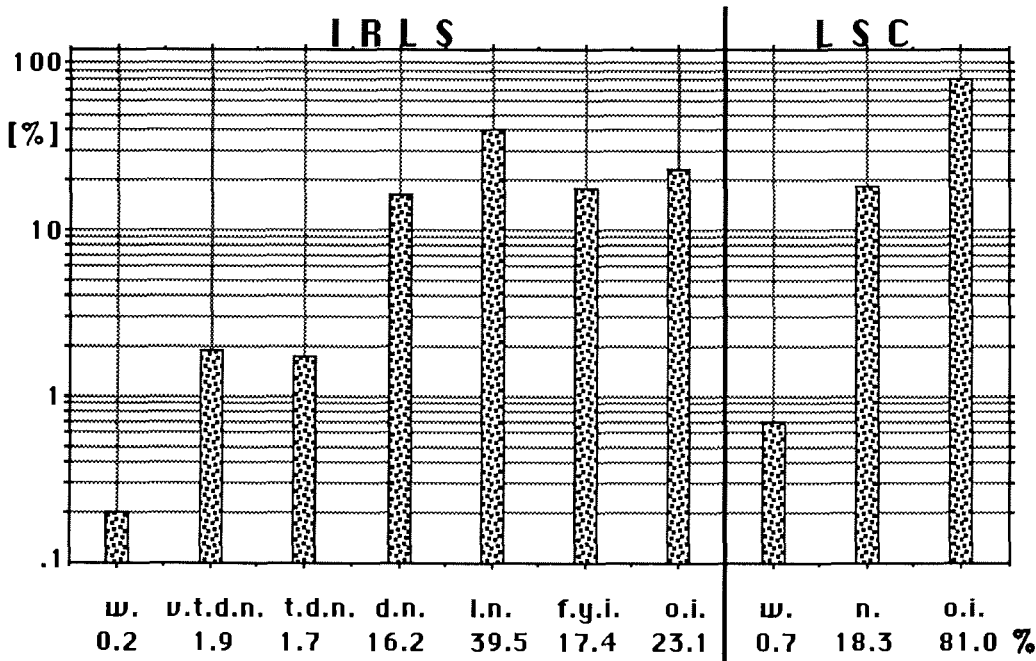


Figure 23: Relative frequencies of different ice types, derived from *IRLS* (left) and the *LSC* (right) data. The numbers beneath the figure give the calculated percentages and refer to figure 22. Notation: w. - water, v.t.d.n. - very thin dark nilas, t.d.n. - thin dark nilas, d.n. - dark nilas, l.n. - light nilas, o.i. old snow covered ice, n. nilas.

however, significantly affect the surface temperature, unless the snow thickness exceeds some 5 to 10 cm. Figure 23 supports this finding. The relative frequencies of 6 different ice types are presented on the left. Surface temperatures decrease from very thin dark nilas (v.t.d.n.) to old snow covered ice (o.i.). The percentage of snow-covered floes from the LSC-data overestimates the area of old ice significantly. More than 75 % of the sea-ice is new ice or nilas, marked by a surface temperature much higher than that of the snow covered thick ice floes in the upper right and the lower left part of Figure 22.

Camera data are obtained during 190 flight legs from heights between 30 m and 3000 m. The total area scanned is 3200 km². Each flight leg is subdivided into single images of 1024 lines x 256 rows, corresponding to a length of about 1.5 km in the flight direction and a width of the aircraft altitude. After correction for vignettation an interactive dynamic threshold method is applied to all images to identify water, nilas and ice.

The mean percentages and areas of three classes at the end of the experiment are

water	2.9 %	92.0 km ²
nilas	4.2 %	134.4 km ²
ice	92.9 %	2968.0 km ²

This distribution is considered as representative for the ice conditions in the marginal ice zone at the end of the winter, since more than 2400 pictures are analyzed for this investigation and the flight legs cover all parts of the marginal ice zone between the inner and the outer region.

6.3. Observation of mesoscale atmospheric structures

Two basic aircraft flight patterns are combined with the release of dropsondes. The development of the convective boundary layer during cold air outbreaks on a scale of roughly 350 km is documented by straight flights of *Polar 4* opposite to the wind of the boundary layer. These flights start at about 78 °N west of Spitzbergen over open water and end near 81 °N over the region with an ice concentration of nearly 100 %. Dropsondes are released at intervals of 50 - 60 km from an altitude of 3000 m. Box patterns with a horizontal scale of 100 km x 100 km are flown near the ice edge. Sondes are released at heights of 1800 m to 2000 m above ground with a horizontal spacing of about 30 km - 60 km. *Polar 2* obtains near-surface turbulent fluxes in the central part of the box. Both patterns provide data for the forcing and validation of mesoscale models.

Cold air outbreaks

Figures 24, 25 and 26 show vertical profiles of potential temperature Θ , specific humidity s and vector plots of horizontal winds from dropsonde data on March 4, 10 and 11.

In all cases the profiles are similar. The initially stably stratified air moves southward over the ocean and heats up. A convective boundary layer with well organized convective rolls develops south from the ice edge.

Satellite images as well as cloud observations from the aircraft show that rolls are clearly developed on March 4 and 10, but not on March 11. Convective layers develop similarly, however. The capping inversion rises almost identically on March 10 and 11 and the Θ -profiles observed at these two days at the same geographic position agree very well. Obviously the convective layer is stationary for a period of nearly 24 hours with respect to temperature.

The wind fields on March 10 and 11 are similar. In both cases the inversion layer height is clearly marked by a change of wind direction. This can be explained by two combined effect of two processes. The **differential heating** over the ice and water causes the horizontal temperature gradients from north to south in the convective layer and within the inversion layer. Therefore the related thermal wind is perpendicular to the temperature gradient, i.e. from west to east, and causes the geostrophic wind to turn to the right with increasing height. **Strong mixing** as the

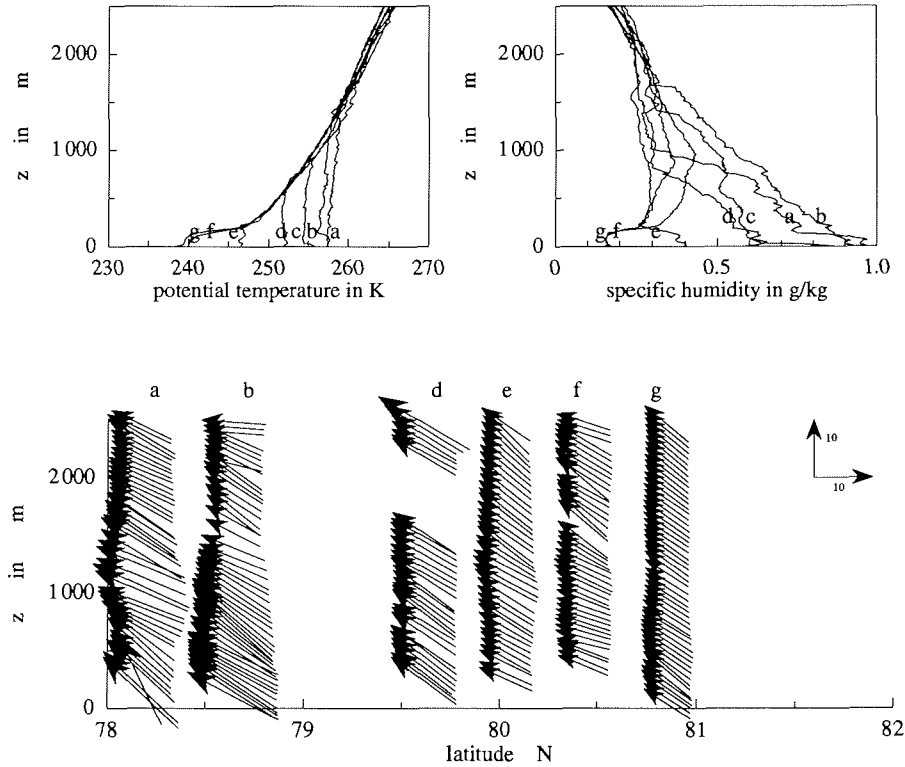


Figure 24: Dropsonde temperature, humidity and wind profiles on March 4. The wind profiles are placed at the release positions of the sondes.

second process acts to distribute the mean momentum homogeneously throughout the layer. The wind shear, therefore, remains confined to the capping inversion layer. A comparison with the aircraft measurements shows that the sondes tend to underestimate changes of wind direction. Wind vectors on March 4 differ from those obtained on March 10 and 11 with respect to both magnitude and shear. A jet like structure with maximum wind speeds of 15 m/s near the ground is observed. In contrary to the other days only a slight change of wind direction is present.

On March 10 and 11 the profiles of specific humidity s also develop similarly. Throughout the whole convective layer s decreases with height on both days. Within the well mixed cloud layer the decrease of s with height is due to condensation of water vapour to liquid water or sublimation to ice. The sublimation process seems to be dominant, since the temperatures are around -20°C and the measured humidities in clouds are close to saturation over an ice surface, but are too low for saturation over water.

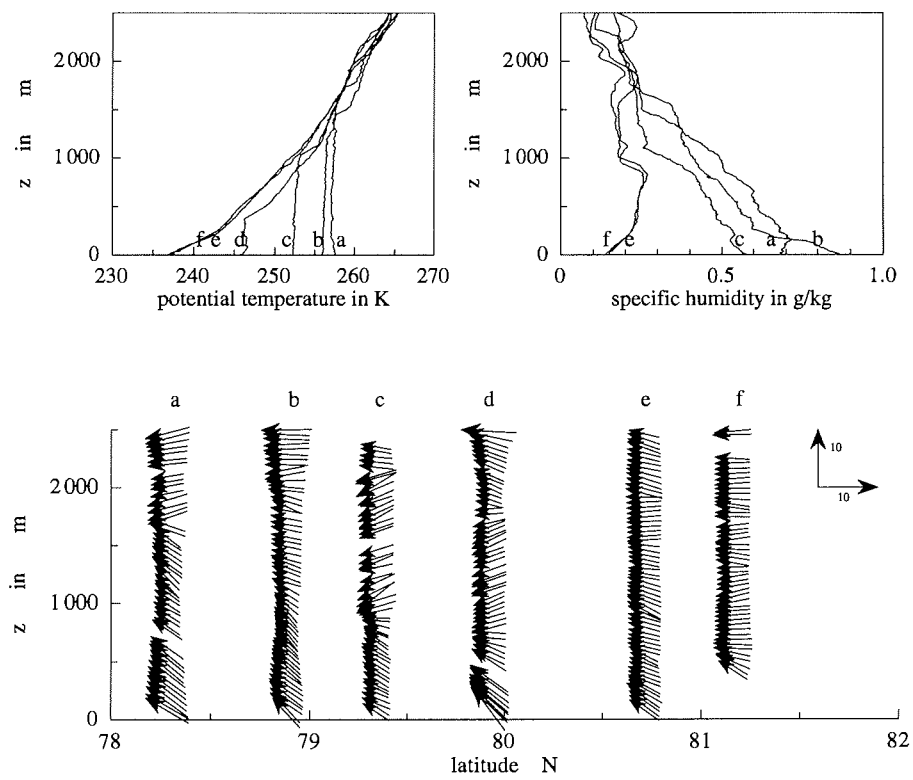


Figure 25: Dropsonde temperature, humidity and wind profiles on March 10. The wind profiles are placed at the release positions of the sondes.

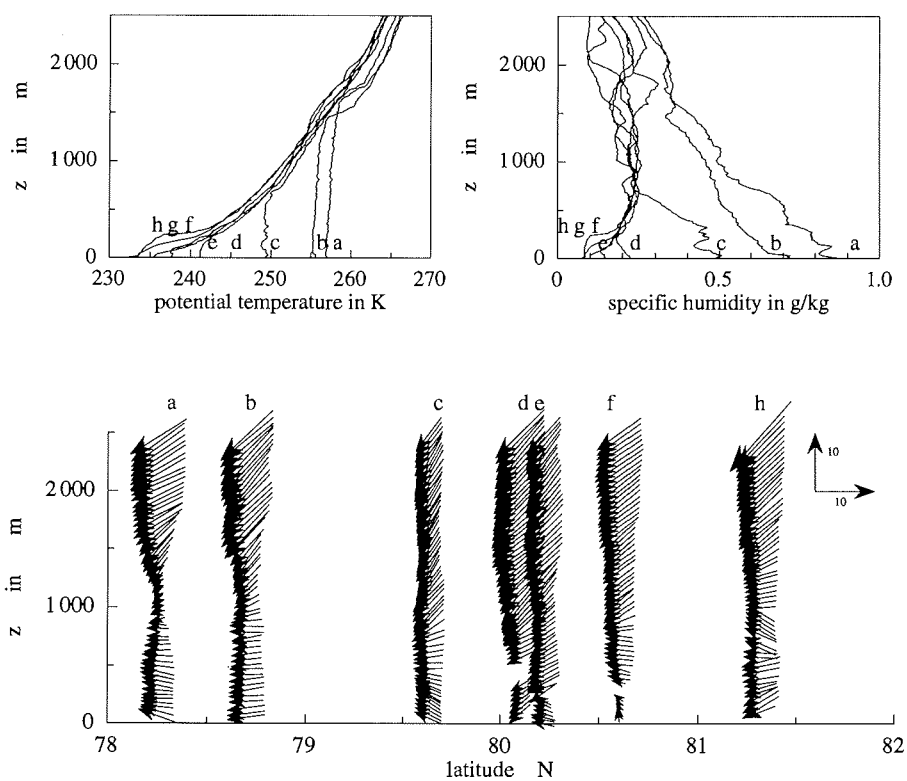


Figure 26: Dropsonde temperature, humidity and wind profiles on March 11. The wind profiles are placed at the release positions of the sondes.

Three dimensional mesoscale structures at the ice margin

Four flights are carried out under different synoptic situations and with different ice conditions. Results obtained from the drop sondes on March 25 are discussed in the following. Drop sondes are released on the peripheries of two boxes. A descent and ascent of *Polar 4* follows each release. Profiles of temperature, humidity and wind are thus available from sondes and *Polar 4*. Additionally *Polar 2* is operating in the inner box close to the ground so that turbulence measurements are available too. The flight tracks, ice concentrations and cloud base and top information is shown in Fig. 27.

The box margins are arranged along and perpendicular to the mean wind direction. Ice concentration isolines run from northwest to southeast. In the northeastern part of the box ice concentration is 100 %, whereas no ice is observed in the southwestern part of the box.

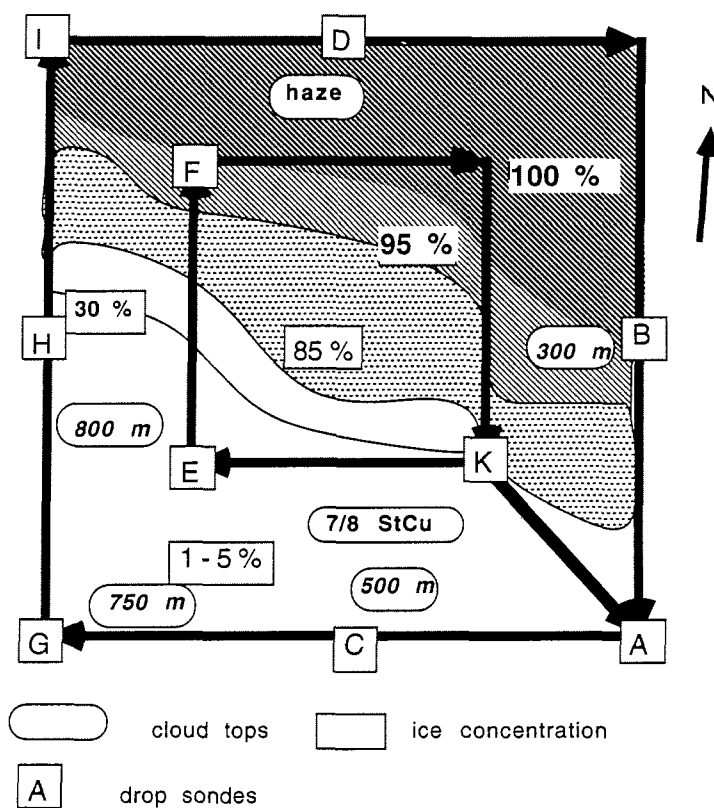


Figure 27: The "double box" flight pattern on March 25, 1993. The capital letters denote the positions and order of dropsonde releases. Ice concentration and cloud information is schematic.

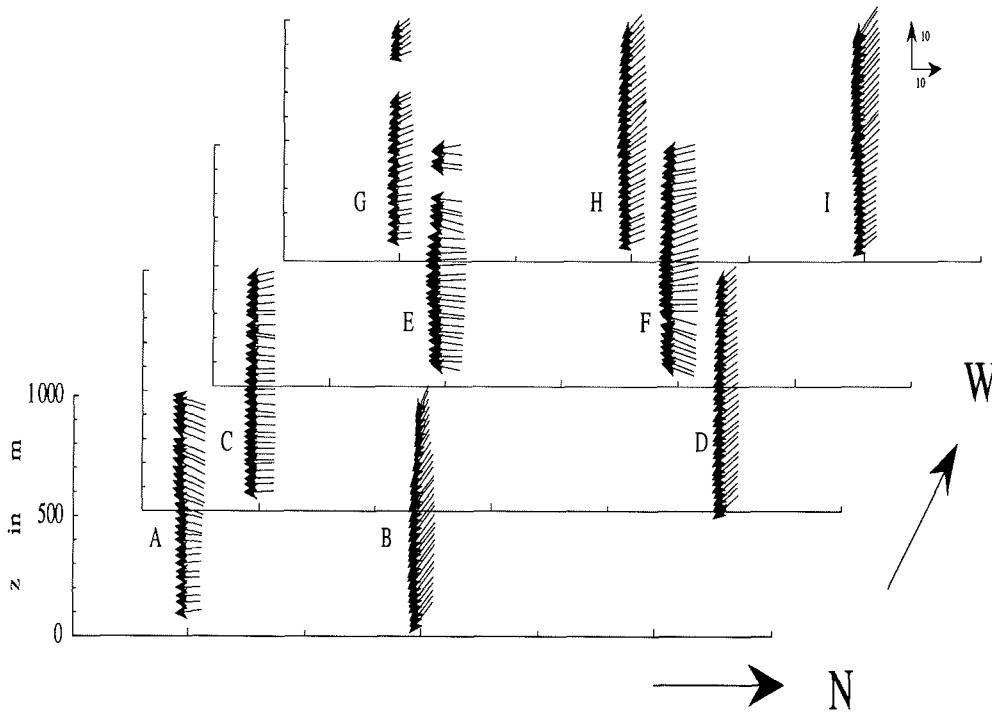


Figure 28: Dropsonde wind profiles on March 25. The profiles are placed such that the lower right corners coincide with the release positions of the sondes.

part. The observed cloud coverage is closely related to the ice concentration. In the north with $I_C > 95\%$ no clouds but arctic haze is present. Convective clouds with tops rising along the flow develop, where leads and open water allow for significant heat and moisture supply from below. A sharp increase of cloud tops is observed near the southern edge. Within a few km cloud tops increase from 500 to 750 m. The cloud basis is close to the ground all over the total box.

The temperature profiles (Fig. 29) show a temperature inversion below the cloud tops in the southern part of the box. Profiles of specific humidity are displayed in Fig. 30. Most profiles show s decreasing with height within the convective layer indicating that condensation or sublimation takes place. In contrast to the data of March 10 and 11, a minimum values of s appears at the inversion.

Two sondes are released at the same geographic position, namely the southeastern corner of the box, with a time lag of roughly 3 hours. Thus the condition of

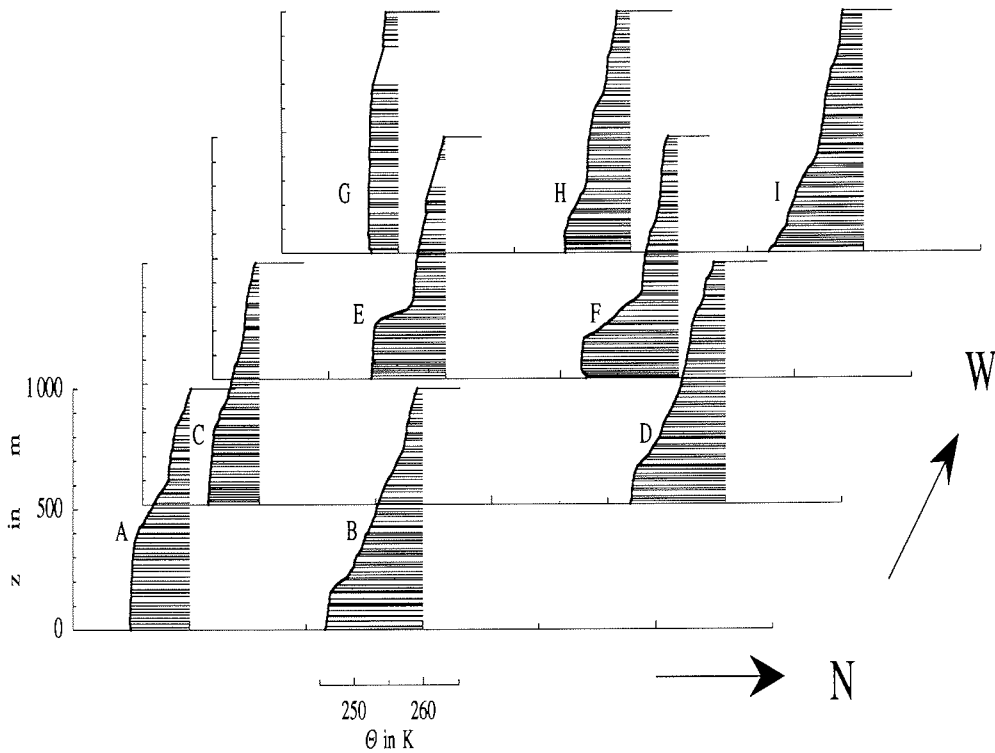


Figure 29: Dropsonde temperature profiles on March 25. The profiles are placed such that the lower right corners coincide with the release positions of the sondes.

stationarity can be checked. The temperatures and humidity profiles from the two sondes agree very well. Fig. 28 displays wind variations within the box. The mean wind direction is from north but there are deviations of roughly 50 degrees near the ground. One of the profiles in the eastern part reveals a change of wind direction by 90 degrees above the inversion. This profile is probably influenced by the orography of Spitzbergen. Wind speed variations are generally small, but some show a jet-like structure as on March 4. Changes of wind direction with height tend to be underestimated by the sondes. On March 25, however, the aircraft observed wind vectors also reveal only small variations in the vertical.

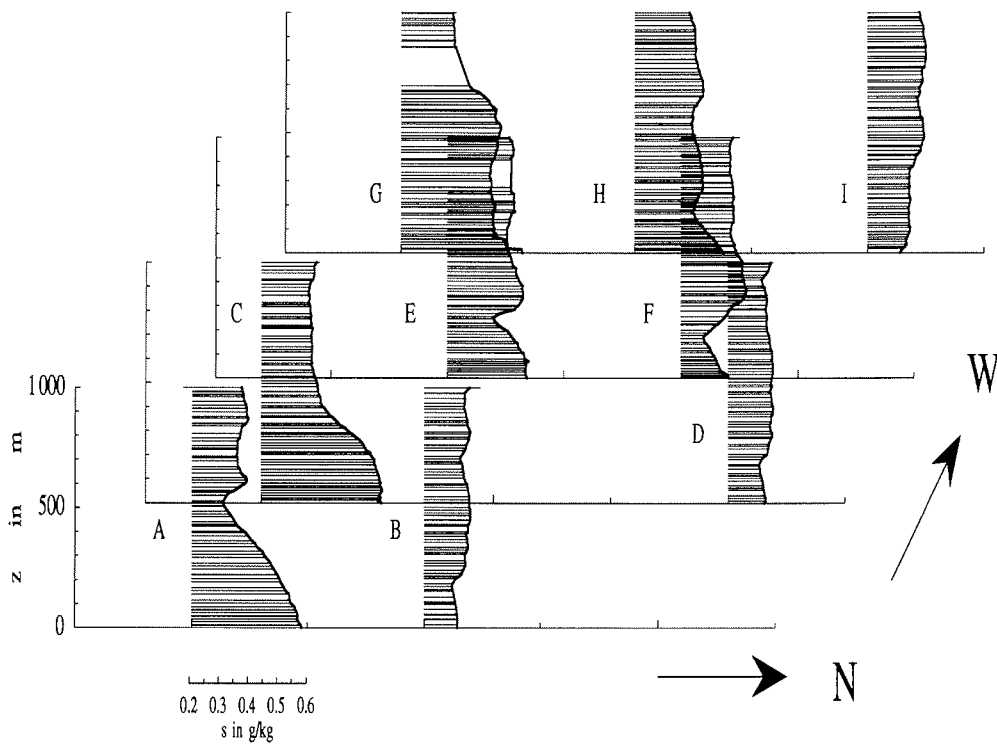


Figure 30: Dropsonde humidity profiles on March 25. The profiles are placed such that the lower right corners coincide with the release positions of the sondes.

6.4. Comparison of ERS I SAR-data and digital camera data

The locations of the SAR-scenes from the ERS I passes during REFLEX II were known during the experiment. The *LSC*, the *IRLS*, the Laser altimeter and the KT4 were used to obtain related surface observations.

An example of intercomparisons is displayed in Figs. 31 to 33. Fig. 31 shows the NOAA-image (Channel 4) of the region, where the cold sea-ice surfaces and the high cirrus clouds in the southwest appear light, whereas the cloud-free oceans are dark and low-level clouds are light grey. The region to the northwest of Spitzbergen marks a SAR scene obtained on the same day. The uncalibrated SAR quicklook data with pixel resolution of 100 m x 100 m were transferred to Longyearbyen via telecommunication. Certain graphical output from these data was transported by *Polar 2* to RV *Polarstern* and used as a basis for glaciological field work.

Fig. 32 shows a subregion of the full SAR-scene, which were also covered by *LSC* and *IRLS*-observations. The light pixels with intense backscatter roughly correspond to the cold ice surfaces in the upper part of the *IRLS*-image. These floes are rather thick and snow covered. In the lower part the surface appears warmer (*IRLS*) and the ice smoother (SAR). This is due to the presence of thin ice of only some 50 cm thickness. From ground observations it is known, that most of this ice formed in the days before the observation. The *LSC*-image in the visible well reflects similar contrasts in the left part of the figure, whereas the surface is masked by sea fog and haze to the right. The *IRLS*-data therefore provide more homogeneous intercomparison data than the *LSC*-images, which are sensitive to day-light conditions and ground visibility.

The displayed band of SAR-, *LSC*- and *IRLS*-data includes the position of RV *Polarstern* (see Fig. 33). The vessel in the upper middle of the figure appears dark and cold. The *IRLS*-image reflects many details of the surface temperature and allows the thin ice to be distinguished from a newly formed lead near the bottom of the figure.

1000 km x 1500 km

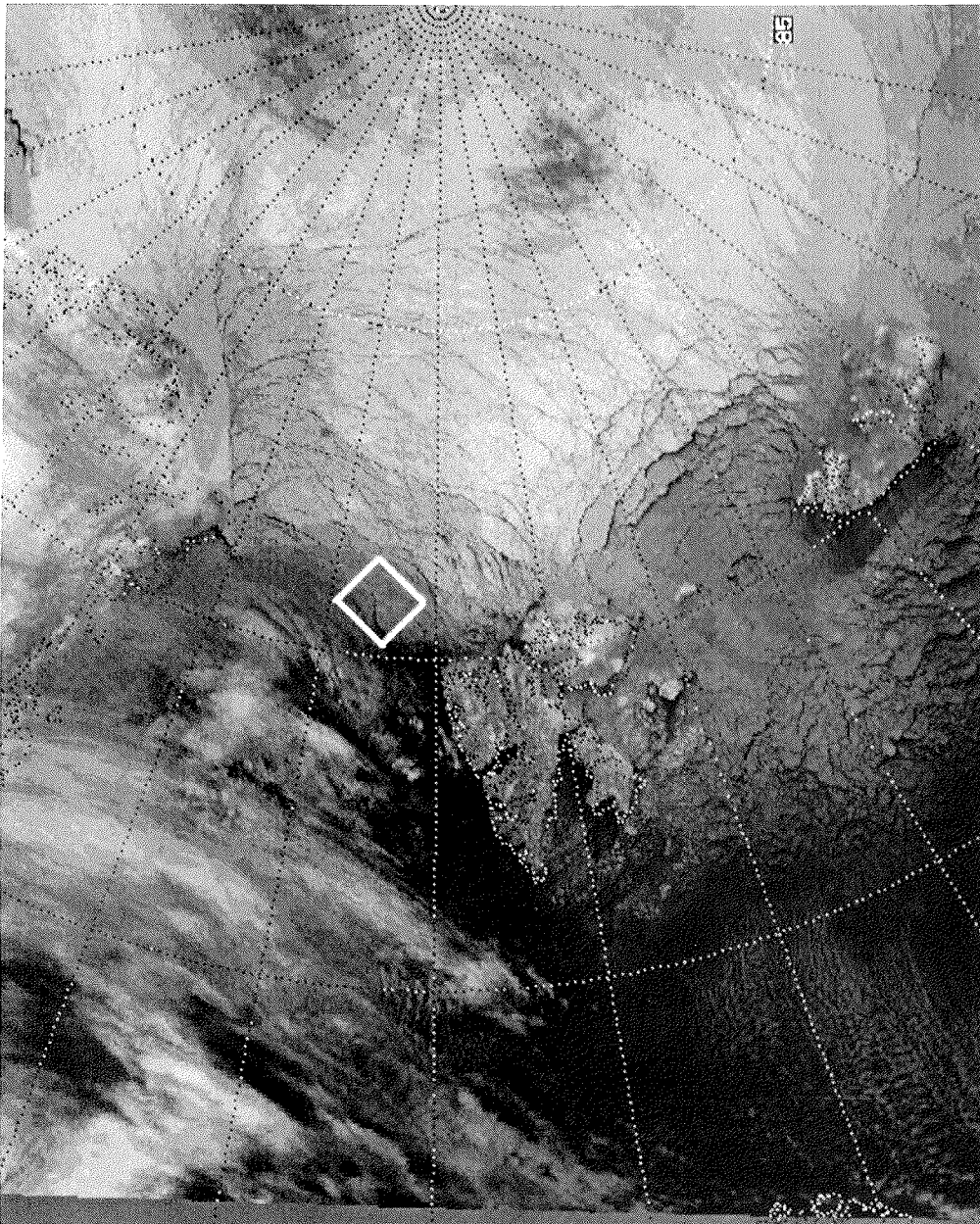


Figure 31: A NOAA-11 image in the thermal infrared (channel 4), obtained on March 12, 1993. The box near the ice margin indicates the position of a scene obtained by the SAR-instrument onboard the ERS-I.

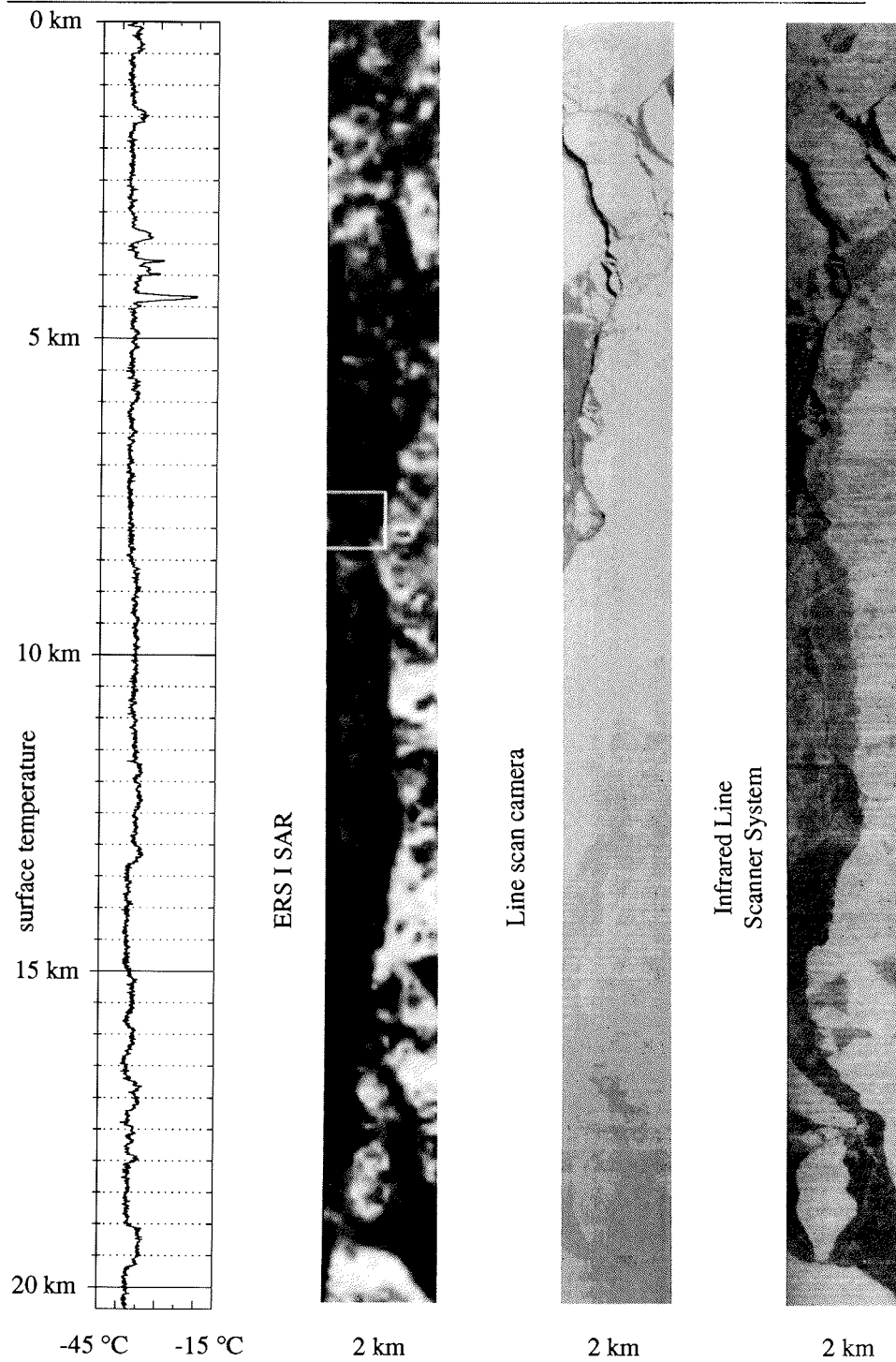


Figure 32: Part of a SAR-scene obtained on March 12, 1993, and related *IRLS*- and *LSC*-data. KT4-surface temperature data in the middle of the band are displayed as well.

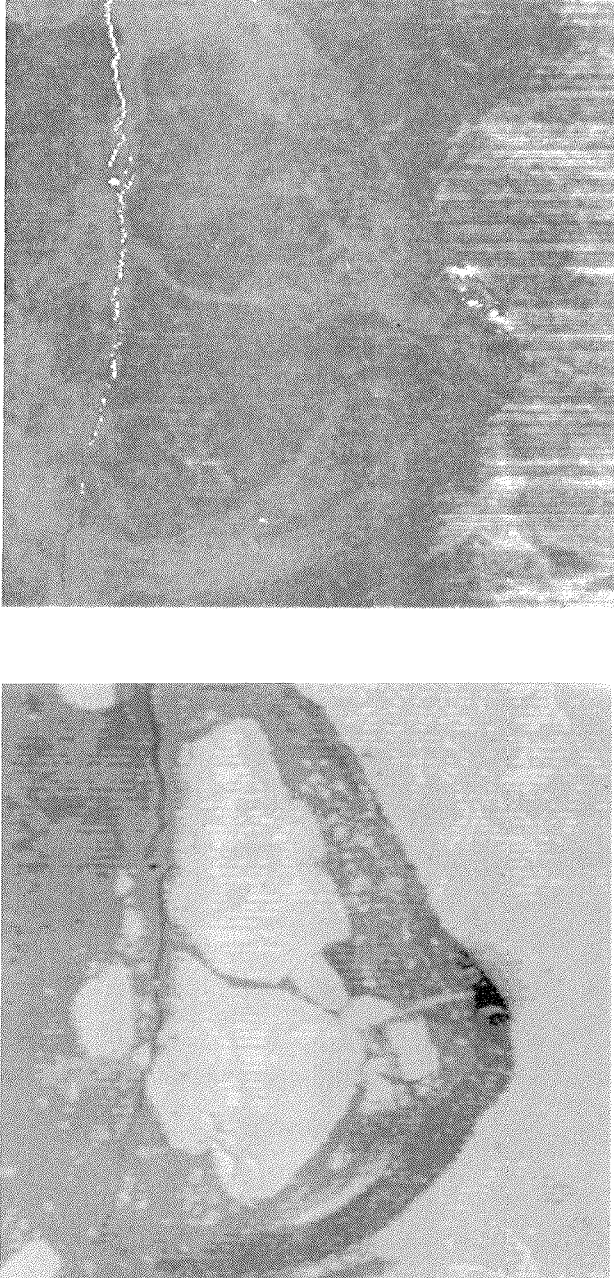


Figure 33: *IRLS*- (top) and *LSC*-data in the vicinity of RV *Polarstern* obtained on March 12, 1993.

7. References

- Albrecht, B., Poellot, M. and S. K. Cox, 1974: Pyrgeometer measurements from aircraft, *Rev. Sci. Instrum.*, 45, A1 - A6.
- Bochert, A., 1992: *RECONOFAX* Systemhandbuch, Alfred-Wegener-Institut für Polar- und Meeresforschung, 1992.
- Bochert, A. and C. Wamser, 1993: The use of airborne line scanner systems for the detection of sea ice structure. accepted by *The Atmosphere - Ocean System*.
- Hartmann, J., Kottmeier, Ch., Wamser, C. and E. Augstein, 1993: Aircraft measured atmospheric momentum heat and radiation fluxes over Arctic Sea Ice. *J. Geophys. Res.*, submitted for publication.
- Hartmann, J., Kottmeier, Ch. and C. Wamser, 1992: Radiation and Eddy Flux Experiment 1991 (REFLEX I). *Ber. Polarforsch.*, 105.
- Kottmeier, Ch., 1993: *User Handbook Polar Aircraft*, Alfred-Wegener-Institut für Polar- und Meeresforschung, 1993.
- Viehoff, T., Eicken, H., Ramseier, R. and P. Wadhams, 1993: Sea ice conditions during ARK IX/1a,b with RV "Polarstern": Shipboard observations and satellite imagery. *Berichte aus dem Fachbereich Physik*, Report 43, Alfred-Wegener-Institut für Polar- und Meeresforschung, 1993.
- Vörsmann, P., Friederici, B. and A. M. Hoff, 1989: METEOPOD – ein flugzeuggestütztes Turbulenzmeßsystem, *Promet* 1/2 1989, 57-64.

8. Acknowledgements

The pilots of *Polar 2* and *Polar 4*, the engineering and technical staff during REFLEX II fulfilled their tasks with great care. The local authorities in Svalbard helped to overcome many problems due to unfavourable weather conditions. We appreciate the good cooperation with the participants of the simultaneous experiment ARKTIS 93, both with respect to the flight activities from Longyearbyen and to the weather information received from the vessels "Polarstern", "Valdivia" and "Professor Multanovsky".

